

METALLIC MEAN WANG TILES II: THE DYNAMICS OF AN APERIODIC COMPUTER CHIP

SÉBASTIEN LABBÉ

ABSTRACT. We consider a new family $(\mathcal{T}_n)_{n \geq 1}$ of aperiodic sets of Wang tiles and we describe the dynamical properties of the set Ω_n of valid configurations $\mathbb{Z}^2 \rightarrow \mathcal{T}_n$. The tiles can be defined as the different instances of a square shape computer chip whose inputs and outputs are 3-dimensional integer vectors. The family include the Ammann aperiodic set of 16 Wang tiles and gathers the hallmarks of other small aperiodic sets of Wang tiles. Notably, the tiles satisfy additive versions of equations verified by the Kari–Culik aperiodic sets of 14 and 13 Wang tiles. Also configurations in Ω_n are the codings of a \mathbb{Z}^2 -action on a 2-dimensional torus like the Jeandel–Rao aperiodic set of 11 Wang tiles. The family broadens the relation between quadratic integers and aperiodic tilings beyond the omnipresent golden ratio as the dynamics of Ω_n involves the positive root β of the polynomial $x^2 - nx - 1$, also known as the n -th metallic mean. We show the existence of an almost one-to-one factor map $\Omega_n \rightarrow \mathbb{T}^2$ which commutes the shift action on Ω_n with horizontal and vertical translations by β on \mathbb{T}^2 . The factor map can be explicitly defined by the average of the top labels from the same row of tiles as in Kari and Culik examples. The proofs are based on the minimality of Ω_n (proved in a previous article) and a polygonal partition of \mathbb{T}^2 which we show is a Markov partition for the toral \mathbb{Z}^2 -action. The partition and the sets of Wang tiles are symmetric which makes them, like Penrose tilings, worthy of investigation.

CONTENTS

1. Introduction	1
2. Statements of the main results	5
3. Preliminaries on dynamical systems, subshifts and Wang shifts	10
4. The family of metallic mean Wang tiles	13
5. The θ_n -chip and metallic mean Wang tiles	17
6. Equations satisfied by the Wang tiles and their tilings	20
7. Valid tilings obtained from floors of linear forms	23
8. An explicit factor map	30
9. Isomorphism with a toral \mathbb{Z}^2 -rotation	33
10. Renormalization and Rauzy induction of \mathbb{Z}^2 -rotations	39
References	44

1. INTRODUCTION

Turing machines can be encoded into a finite set of Wang tiles (unit squares with labelled edges) in such a way that the Turing machine does not halt if and only if there exists a tiling of the plane by translated copies of the tiles respecting the condition that the common edge of adjacent tiles have the same label [Ber66], see also [Rob71, Oll08, JV20]. As a consequence, the existence of a valid tiling of the plane with a given finite set of Wang tiles (called the domino problem) can not be

Date: March 6, 2024.

2020 Mathematics Subject Classification. Primary 52C23; Secondary 37B51, 37A05, 11B39.

Key words and phrases. Wang tiles and aperiodic tiling and monotile and renormalization and metallic mean.

decided by an algorithm. Indeed, if the domino problem were decidable, we could use the algorithm solving the domino problem to solve the halting problem, which is a contradiction [Tur36].

Therefore, we can think of Wang tiles as if their tilings are computing something. As observed by Wang, the undecidability of the domino problem implies the existence of aperiodic sets of Wang tiles [Wan61] which has developed into an active subject of study with application to the theory of quasicrystals [GS87, Sen95, BG13, BG17]. Thus, sets of Wang tiles (and their computations) can be classified into three cases [JR21]:

- **Finite:** the Wang tiles do not tile the plane,
- **Periodic:** the Wang tiles tile the plane and one of the valid tilings is periodic,
- **Aperiodic:** the Wang tiles tile the plane and none of the valid tilings are periodic.

The finite cases can be associated with computations that halt. The periodic cases can be associated with computations that do not halt and fall into an infinite loop. The aperiodic cases can be associated with computations that do not halt and never repeat.

For applications, computations that halt are usually preferred over computations that loop forever. Among computations that halt, the description of those “busy beavers” [Bra88, Aar20] running for the maximum number of steps before halting is an open question even for Turing machines made of only 5 rules [OEI23]. In this article, we are interested in the description of computations that do not halt and never repeat. We focus on those that happen to be performed by small aperiodic sets of Wang tiles. We aim to reveal their links with dynamical systems and the coding of their orbits.

The Kari–Culik outliers. The smallest sets of aperiodic Wang tiles until 2015 were discovered by Kari and Culik in 1996. Kari [Kar96] proved that a well-chosen set of 14 Wang tiles admits tilings of the plane, and that none of them is periodic. The proof that they are not periodic is cleverly short. It is based on an arithmetic interpretation of the edge labels of the Wang tiles. The tiles have labels $r, t, \ell, b \in \mathbb{Q}$ satisfying an equation

$$(1.1) \quad \begin{array}{ccc} & t & \\ \ell & \square & r \\ & b & \end{array} \quad qt + \ell = b + r$$

for some $q \in \mathbb{Q}$. We may interpret the Wang tile as a computation (the multiplication by q) with value t as an input and b as an output. The value ℓ is a carry input on the left and r is a carry output on the right. Kari [Kar96] proposed a set of four tiles satisfying (1.1) with $q = 2$ and ten tiles with $q = \frac{2}{3}$. The proof of the non-existence of a periodic tiling with those 14 tiles uses the fact that the equation $2^m 3^n = 1$ has only one solution over the integers ($m = n = 0$). Based on the same idea, Culik [Cul96] proposed a smaller aperiodic set of 13 tiles (four tiles satisfying (1.1) with $q = 3$ and nine tiles with $q = \frac{1}{2}$). Note that generalizations of Kari–Culik tilings exist [ENP07] and that further results were obtained about their entropy [DGG17] and on a minimal subsystem [Sie17].

Among aperiodic tilings of the plane by Wang tiles, Kari and Culik sets seem like outliers. The aperiodicity of Penrose tiles [Pen79], Berger tiles [Ber66], Robinson tiles [Rob71], Knuth tiles [Knu69], Ammann tiles [GS87, AGS92] can be explained by the hierarchical decomposition of their tilings. Often, aperiodic tilings have a self-similar structure [Sol97, Sol98, PS01, Pra99, AA20] and this is the case for recently discovered aperiodic geometrical tiles [ST11, SMKG23a, SMKG23b]. However, Kari and Culik tilings have positive entropy. Thus, they are not self-similar and do not possess a hierarchical decomposition [DGG17]. Moreover, except some extensions of Kari and Culik sets [ENP07, §6], no other known aperiodic sets of tiles satisfy equations explaining their non-periodicity.

The Jeandel–Rao example. For almost twenty years, the Kari and Culik sets of Wang tiles were the smallest known aperiodic sets of Wang tiles. In 2015, Jeandel and Rao performed an exhaustive search on all sets of Wang tiles of cardinality up to 11 [JR21] and proved that sets of Wang tiles of cardinality at most 10 either do not tile the plane or tile the plane and one of the valid tilings is periodic. Moreover, they provided a list of 36 sets of 11 Wang tiles considered to be candidates for being aperiodic. One of candidates was intriguing because Fibonacci numbers appeared in the structure of the transducers involved in the computation of valid tilings. Jeandel and Rao focused on the intriguing candidate, shown in Figure 1, and they proved it to be aperiodic. We identify the set of valid configurations over these 11 tiles as the Jeandel–Rao Wang shift.

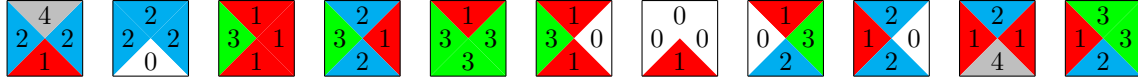


FIGURE 1. The Jeandel–Rao aperiodic set of 11 Wang tiles.

In [Lab21a], it was proved that a minimal subshift within the Jeandel–Rao Wang shift is the coding of a dynamical system defined by the following \mathbb{Z}^2 -action R_0 on the 2-dimensional torus \mathbb{R}^2/Γ_0 , where $\Gamma_0 = \begin{pmatrix} \varphi & 1 \\ 0 & \varphi+3 \end{pmatrix} \mathbb{Z}^2$ is a lattice in \mathbb{R}^2 involving the golden ratio $\varphi = \frac{1+\sqrt{5}}{2}$:

$$R_0 : \mathbb{Z}^2 \times \mathbb{R}^2/\Gamma_0 \rightarrow \mathbb{R}^2/\Gamma_0$$

$$(\mathbf{k}, \mathbf{x}) \mapsto \mathbf{x} + \mathbf{k}.$$

The symbolic coding is obtained through a polygonal partition \mathcal{P}_0 of a fundamental domain of \mathbb{R}^2/Γ_0 . The partition was proved to be a Markov partition for R_0 after comparing the substitutive structure computed from the Rauzy induction of R_0 and \mathcal{P}_0 [Lab21b] with the substitutive structure of the associated Wang shift [Lab19, Lab21c].

Intuitively, this means that the Jeandel–Rao Wang tiles shown in Figure 1 correspond to computing the orbit of points in the plane \mathbb{R}^2 under the translations by $+1$ horizontally and $+1$ vertically modulo the lattice Γ_0 . How come this is possible is still a mystery. The link between the 11 Jeandel–Rao Wang tiles themselves and the golden ratio or toral rotation R_0 remains unclear. Unlike the Kari example, the values 0, 1, 2, 3, 4 of the labels of the Jeandel–Rao Wang tiles are five distinct symbols rather than arithmetic values. They do not satisfy a known equation. The following questions can be raised.

Question 1. *Let \mathcal{T} be a set of Wang tiles such that the Wang shift $\Omega_{\mathcal{T}}$ is aperiodic. Can we replace the labels of the tiles in \mathcal{T} by arithmetic values in such a way that an equation similar to (1.1) is satisfied?*

Question 2. *If Question 1 is answered for a set \mathcal{T} of Wang tiles, can we use the equations satisfied by the tiles to directly prove that the Wang shift $\Omega_{\mathcal{T}}$ is aperiodic following the short arithmetical argument for the nonperiodicity of Kari’s tile set?*

Solving Question 1 for Jeandel–Rao Wang tiles would improve our understanding of the Jeandel–Rao Wang shift. Hopefully it would allow to generate similar examples maybe not related to the golden ratio. Remember that the computations made by Jeandel and Rao took one year using 100 cpus to explore exhaustively the sets of 11 Wang tiles [JR21]. Finding new examples by exploring all sets of 12, 13 or 14 Wang tiles becomes soon out of reach. We need to understand what is happening in order to find other examples and characterize them. In general, we may ask the following question.

Question 3. *For which invertible matrix $M \in \text{GL}_2(\mathbb{R})$ does there exist a set of Wang tiles \mathcal{T} such that the Wang shift $\Omega_{\mathcal{T}}$ is isomorphic, as a measure-preserving dynamical system, to the toral \mathbb{Z}^2 -rotation $R : \mathbb{Z}^2 \times \mathbb{T}^2 \rightarrow \mathbb{T}^2$ defined by $R^k(\mathbf{x}) = \mathbf{x} + M\mathbf{k}$ on the 2-dimensional torus $\mathbb{T}^2 = (\mathbb{R}/\mathbb{Z})^2$?*

This article. In this article, we demonstrate that Kari and Culik tilings are not a complete oddity within aperiodic set of tiles. In particular, we show for the first time that substitutive aperiodic sets of Wang tiles can also satisfy equations and even be defined by them. We provide an answer to Question 1 for the Ammann set of 16 Wang tiles [GS87] as well as a family of aperiodic Wang tiles associated with the metallic mean numbers, the positive roots of the polynomials $x^2 - nx - 1$ where $n \geq 1$ is a positive integer.

The labels of the Wang tiles are not numbers like in Kari and Culik sets, but rather integer vectors. The equations satisfied by the tiles are derived from a deterministic function that expresses a relation between the labels of the Wang tiles. The deterministic function provides an independent definition of the family of metallic mean Wang shifts. The family $(\Omega_n)_{n \geq 1}$ of metallic mean Wang shifts was introduced separately in [Lab23a] where it was shown to be self-similar, aperiodic and minimal. Here, in this second article on the metallic mean Wang tiles, we study its dynamical properties from the point of view of the instances of an aperiodic computer chip.

For every integer $n \geq 1$, we show that valid configurations in Ω_n are computing the orbits of a dynamical system defined by a \mathbb{Z}^2 -action on the 2-dimensional torus \mathbb{T}^2 . The dynamical system is defined by horizontal and vertical translation on \mathbb{T}^2 by the n -th metallic mean modulo 1. As for the Jeandel–Rao Wang shift [Lab21a], the proof is based on a polygonal partition of \mathbb{T}^2 which we prove is a Markov partition for the toral \mathbb{Z}^2 -action. We prove the existence of an almost one-to-one factor map $\Omega_n \rightarrow \mathbb{T}^2$.

The factor map can be defined by taking averages of the dot product involving the top labels of the Wang tiles in the biinfinite row of tiles passing through the origin in a configuration. The existence of the factor map proves that the average changes from row to row by an irrational rotation by the n -th metallic mean number. This can be seen as an additive version of a multiplicative phenomenon known for Kari–Culik tilings. Recall that the average of top label values along a row is at the heart of Kari and Culik’s construction of aperiodic tilings where the average change by a rational multiplication from row to row [DGG17, Theorem 6].

The polygonal partition used to encode the toral \mathbb{Z}^2 -action is symmetric and is much more simple to define compared to the Markov partition associated with the Jeandel–Rao Wang shift. Moreover, the label of the polygonal atoms of the partition have a meaning in the sense that they define the linear inequalities describing their boundaries. The symmetry and simplicity of the partition was helpful to extend the family beyond the golden ratio. More work needs to be done to answer Question 1 for Jeandel–Rao tiles because its partition is more complex. The results proved here for the metallic mean Wang tiles should serve as an inspiration to replace the labels of the Jeandel–Rao tiles by integer vectors satisfying equations.

Structure of the article. In Section 2, we state the main results proved in this article. In Section 3, we present preliminary notions on dynamical systems, subshifts and Wang shifts. In Section 4, we recall the definition of the family of metallic mean Wang tiles. In Section 5, we show that instances of the θ_n -chip are the metallic mean Wang tiles. This proves Theorem A. In Section 6, we prove Theorem B and we present more equations satisfied by the metallic mean tiles and their tilings. In Section 7, we use the floor function on linear forms to construct valid tilings with the metallic mean Wang tiles and we prove Theorem C. In Section 8, we define an explicit factor map $\Omega_n \rightarrow \mathbb{T}^2$ and we prove Theorem D. In Section 9, we define the partition \mathcal{P}_n for every integer $n \geq 1$ and we show that the metallic mean Wang shift is equal to the symbolic dynamical system defined by the coding of a toral \mathbb{Z}^2 -action by this partition. This shows that Ω_n is isomorphic as measure-preserving dynamical systems to a toral \mathbb{Z}^2 -action. We prove Theorem E

and Theorem F in this section. In Section 10, we compute the renormalization of the partition \mathcal{P}_n and \mathbb{Z}^2 -action R_n using computations performed in SageMath when $n = 3$. We illustrate how the Rauzy induction of \mathbb{Z}^2 -actions and of polygonal partitions can be used to show the self-similarity of the symbolic dynamical system $\mathcal{X}_{\mathcal{P}_n, R_n}$.

Acknowledgments. The author is thankful to Hugo Parlier for his comments on an earlier draft of the introduction during the workshop *Renormalization and visualization in geometry, dynamics and number theory* held at CIRM in Marseille in December 2023. I am thankful to Vincent Delecroix to help me realize that it's not the Birkhoff ergodic theorem which is needed in the proof of Proposition 8.2 but rather simply the Weyl's equidistribution theorem. The author acknowledges funding from France's Agence Nationale de la Recherche (ANR) project CODYS (ANR-18-CE40-0007) and project IZES (ANR-22-CE40-0011).

2. STATEMENTS OF THE MAIN RESULTS

An aperiodic computer chip. For every integer $n \geq 1$, we define a finite subset $V_n \subset \mathbb{N}^3$ of vectors

$$V_n = \{(v_0, v_1, v_2) \in \mathbb{N}^3 : 0 \leq v_0 \leq v_1 \leq v_2 \leq n + 1 \text{ and } v_1 \leq 1\}$$

with nondecreasing entries where the middle entry is at most 1. We introduce a function

$$\theta_n : \begin{array}{ccc} V_n \times V_n & \rightarrow & \mathbb{N}^3 \\ (u_0, u_1, u_2), (v_0, v_1, v_2) & \mapsto & (r_0, r_1, r_2), \end{array}$$

taking two vectors as input and returning one vector. Its image is defined by the rule

$$(2.1) \quad \left\{ \begin{array}{l} r_0 = u_0, \\ r_1 = \begin{cases} v_2 - n & \text{if } u_0 = 0, \\ 1 & \text{if } u_0 = 1, \end{cases} \\ r_2 = \begin{cases} v_1 + u_0 & \text{if } v_0 = 0, \\ u_2 + 1 & \text{if } v_0 = 1. \end{cases} \end{array} \right.$$

For every integer $n \geq 1$, we construct a symmetric θ_n -chip, that is, a computer chip taking as inputs $u \in V_n$ on the left and $v \in V_n$ on the bottom and producing as outputs $\theta_n(u, v)$ on the right and $\theta_n(v, u)$ on the top (see Figure 2).

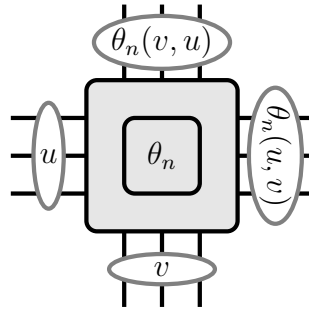
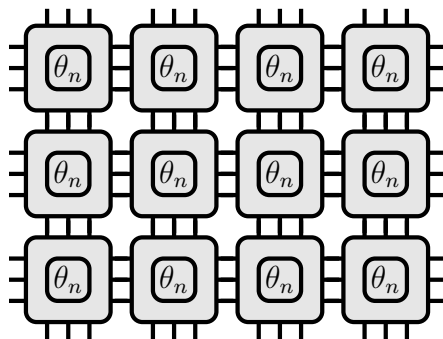


FIGURE 2. The θ_n -chip is a computer chip computing $\theta_n(u, v)$ and $\theta_n(v, u)$ from the left input u and bottom input v .

If $\theta_n(u, v)$ and $\theta_n(v, u)$ are in V_n , then one can use multiple copies of the θ_n -chip and connect them to each other horizontally and vertically into an arbitrarily large rectangular cluster of θ_n -chips (see Figure 3).

FIGURE 3. A rectangular cluster of copies of the θ_n -chip.

The results. We prove in this work the existence of arbitrarily large rectangular clusters of the θ_n -chip all of them performing correct computations. Also we show that no rectangular cluster of the θ_n -chip perform a periodic computation. Thus we say that the θ_n -chip is an **aperiodic computer chip**. Perhaps we can say it is an *aperiodic monochip*, but we can not say it is an *aperiodic monotile* as in [SMKG23a,SMKG23b] because the same chip with different inputs has to be considered a distinct Wang tile. If we consider all possible values of inputs u and v in V_n and if we restrict the outputs to be in the set V_n , then we obtain a finite set of Wang tiles

$$(2.2) \quad \mathcal{C}_n = \left\{ \begin{array}{c} \theta_n(v, u) \\ u \quad \square \quad \theta_n(u, v) \\ v \end{array} \left| u, v \in V_n \text{ such that } \theta_n(u, v), \theta_n(v, u) \in V_n \right. \right\}$$

which is the finite set of all possible instances of the θ_n -chip.

Theorem A. *For every integer $n \geq 1$, the Wang shift $\Omega_{\mathcal{C}_n}$ defined by the θ_n -chip is the n^{th} metallic mean Wang shift Ω_n .*

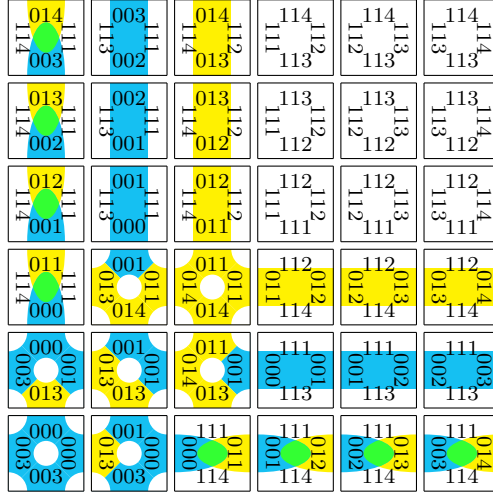
Something unexpected and surprising happens in the proof of Theorem A. The set \mathcal{C}_n of instances of the θ_n -chip is exactly equal to the extended set \mathcal{T}'_n of metallic mean Wang tiles introduced in [Lab23a] in order to prove the self-similarity of Ω_n , see Proposition 5.1.

It was shown in [Lab23a] that the metallic mean Wang shift Ω_n is self-similar, aperiodic and minimal. The n^{th} metallic mean Wang shift Ω_n is defined from a set \mathcal{T}_n of $(n+3)^2$ Wang tiles. When $n=1$, it was observed in [Lab23a] that \mathcal{T}_1 is equivalent to the Ammann set of 16 Wang tiles. An illustration of the set \mathcal{T}_3 is shown in Figure 4 where we represent vectors in V_n as words for economy of space reasons. For instance, the vector $(1, 1, 4)$ is represented as 114.

The next result states that every tiles in \mathcal{C}_n satisfy a system of equations. While the equations associated with Kari's [Kar96] and Culik's [Cul96] aperiodic set of Wang tiles are multiplicative, the ones associated with \mathcal{C}_n are additive. The first of these equations remind of Equation (1.1). Like Kari's and Culik's tiles, these equations behave well with tilings and more equations can be deduced for valid tilings of a rectangle, see Section 6.

Theorem B. *Let $n \geq 1$ be an integer, $d = (0, -1, 1)$ and $e = (1, 0, 0)$. The set of Wang tiles defined by the θ_n -chip satisfy the following system of equations:*

$$\mathcal{C}_n \subseteq \left\{ \begin{array}{c} t \\ \ell \quad \square \quad r \\ b \end{array} \in V_n \times V_n \times V_n \times V_n \left| \begin{array}{l} \langle \frac{1}{n}d, t + \ell \rangle = \langle \frac{1}{n}d, b + r \rangle + \langle e, \ell - b \rangle \\ \langle e, \ell \rangle = \langle e, r \rangle \\ \langle e, b \rangle = \langle e, t \rangle \end{array} \right. \right\}$$


 FIGURE 4. The metallic mean Wang tile set \mathcal{T}_n for $n = 3$.

where $\langle _, _ \rangle$ denotes the canonical inner product of \mathbb{Z}^3 .

Unfortunately, we were unable to use the equations satisfied by the labels of θ_n -chip to show directly the aperiodicity of the Wang shift Ω_n as this is nicely done for Kari and Culik sets of tiles. Thus Question 2 remains open for the family of metallic mean Wang shifts.

Valid tilings in Ω_n can be constructed using the floor function on linear forms. Let $\Lambda_n : [0, 1)^2 \rightarrow \mathbb{Z}^3$ be defined as

$$\Lambda_n(x, y) = \begin{pmatrix} \lfloor y - \beta^{-1} + 1 \rfloor \\ \lfloor \beta^{-1}x + y - \beta^{-1} + 1 \rfloor \\ \lfloor \beta x + y - \beta^{-1} + 1 \rfloor \end{pmatrix}.$$

where β is the n^{th} metallic mean, that is, the positive root of the polynomial $x^2 - nx - 1$. For every $(x, y) \in [0, 1)^2$, let $c_{(x,y)} : \mathbb{Z}^2 \rightarrow \mathcal{T}_n$ be the configuration which maps the position $(i, j) \in \mathbb{Z}^2$ to the Wang tile

$$\begin{array}{ccc} \Lambda_n(\{y+j\beta^{-1}\}, \{x+i\beta^{-1}\}) & & \\ \Lambda_n(\{x+(i-1)\beta^{-1}\}, \{y+j\beta^{-1}\}) & \square & \Lambda_n(\{x+i\beta^{-1}\}, \{y+j\beta^{-1}\}) \\ \Lambda_n(\{y+(j-1)\beta^{-1}\}, \{x+i\beta^{-1}\}) & & \end{array}$$

where $\{x\} = x - \lfloor x \rfloor$ is the fractional part of a number $x \in \mathbb{R}$.

Theorem C. *Let $n \geq 1$ be an integer. For every $(x, y) \in [0, 1)^2$, the configuration*

$$c_{(x,y)} : \mathbb{Z}^2 \rightarrow \mathcal{T}_n$$

is a valid tiling of the plane by the set of metallic mean Wang tiles \mathcal{T}_n .

This construction reminds of the proof of existence of tilings with Kari and Culik tiles based on the balanced representation of real numbers and first difference of Beatty sequences [Kar96, Cul96], see also [ENP07, Sie17].

In Kari–Culik tilings [Kar96, Cul96], there is a well-defined notion of average [DGG17] of the top tile labels along a bi-infinite horizontal row. The value from one row to the next row is described by a piecewise rationally multiplicative map. In this context, metallic mean Wang shifts also behave

like Kari–Culik tilings. It involves the consideration of the average of specific inner products and irrational rotations instead of multiplications, see Figure 5.

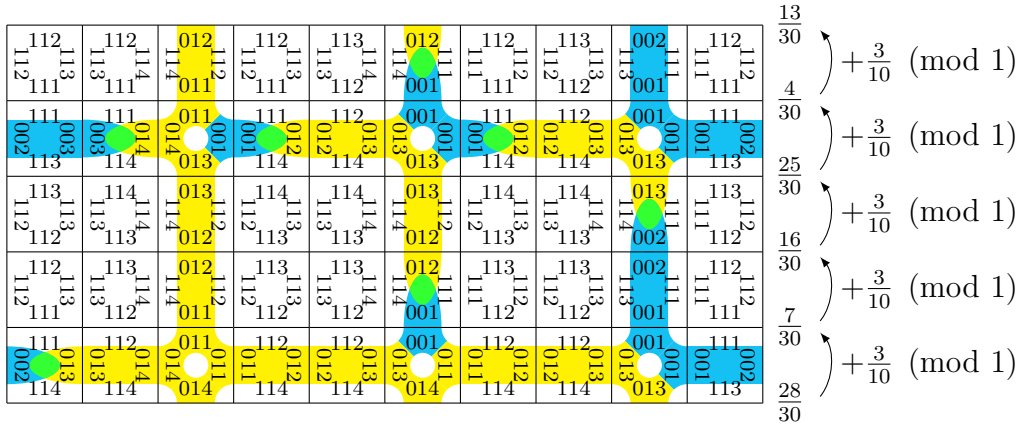


FIGURE 5. A 10×5 valid rectangular tiling with the set \mathcal{T}_n with $n = 3$. The numbers indicated in the right margin are the average of the inner products $\langle \frac{1}{n}d, v \rangle$ over the vectors v appearing as top (or bottom) labels of a horizontal row of tiles and where $d = (0, -1, 1)$. We observe that these numbers increase by $\frac{3}{10} \pmod{1}$ from row to row. The number $\frac{3}{10}$ is equal to the frequency of columns containing junction tiles (a junction tile is a tile whose labels all start with 0). Observe that this is a cylindrical tiling (left and right outer labels of the rectangle match) which simplifies the equations involved because the left and right carries cancel.

We show that the average of the dot products of the vector $\frac{1}{n}d = \frac{1}{n}(0, -1, 1)$ with the top labels of a given row in a valid configuration $\mathbb{Z}^2 \rightarrow \mathcal{T}_n$ in Ω_n is well-defined and takes a value in the interval $[0, 1]$ (see Equation (8.1)). By symmetry of the set \mathcal{T}_n , the same holds for the right labels of a given column. By considering the row and column going through the origin of a configuration, the two averages define a map $\Phi_n : \Omega_n \rightarrow \mathbb{T}^2$ (see Equation (8.2)). We prove that this map is a factor map from the Wang shift to the 2-torus.

Theorem D. *Let $n \geq 1$ be an integer and Ω_n be the n^{th} metallic mean Wang shift. The map $\Phi_n : \Omega_n \rightarrow \mathbb{T}^2$ is a factor map, that is, it is continuous, onto and commutes the shift $\mathbb{Z}^2 \xrightarrow{\sigma} \Omega_n$ with the toral \mathbb{Z}^2 -rotation $\mathbb{Z}^2 \xrightarrow{R_n} \mathbb{T}^2$ by the equation $\Phi_n \circ \sigma^k = R_n^k \circ \Phi_n$ for every $k \in \mathbb{Z}^2$ where*

$$\begin{aligned} R_n : \mathbb{Z}^2 \times \mathbb{T}^2 &\rightarrow \mathbb{T}^2 \\ (k, x) &\mapsto R_n^k(x) := x + \beta k \end{aligned}$$

and $\beta = \frac{n + \sqrt{n^2 + 4}}{2}$ is the n^{th} metallic mean, that is, the positive root of the polynomial $x^2 - nx - 1$.

This is an analogue of a result known for Kari and Culik aperiodic Wang tilings which satisfy equations involving balanced representations of real numbers and orbits of piecewise rationally multiplicative maps, see also Theorem 16 in [ENP07] and Proposition 3 in [Sie17]. Here the result applies to all of the configurations in the Wang shift Ω_n .

Theorem D implies that Ω_n is aperiodic because β is irrational and R_n is a free \mathbb{Z}^2 -action (see for instance Lemma 5.2 in [Lab21a]). Note that since $\beta - \beta^{-1} = n$, we have $\beta = \beta^{-1} \pmod{1}$.

Applying the results already proved for Jeandel–Rao Wang shift [Lab21a], we have the following additional properties for the factor map. We refer the reader to the preliminary Section 3 for the notions and vocabulary on topological and measure-preserving dynamical systems that are used in the statement. A similar result holds for Penrose tilings [Rob96].

Theorem E. *The Wang shift Ω_n and the \mathbb{Z}^2 -action R_n have the following properties:*

- (i) $\mathbb{Z}^2 \overset{R_n}{\curvearrowright} \mathbb{T}^2$ is the maximal equicontinuous factor of $\mathbb{Z}^2 \overset{\sigma}{\curvearrowright} \Omega_n$,
- (ii) the factor map $\Omega_n \rightarrow \mathbb{T}^2$ is almost one-to-one and its set of fiber cardinalities is $\{1, 2, 8\}$,
- (iii) the dynamical system $\mathbb{Z}^2 \overset{\sigma}{\curvearrowright} \Omega_n$ is strictly ergodic and the measure-preserving dynamical system $(\Omega_n, \mathbb{Z}^2, \sigma, \nu)$ is isomorphic to $(\mathbb{T}^2, \mathbb{Z}^2, R_n, \lambda)$ where ν is the unique shift-invariant probability measure on Ω_n and λ is the Haar measure on \mathbb{T}^2 .

The proof of Theorem E are based on a polygonal partition \mathcal{P}_n of the torus $\mathbb{T}^2 = \mathbb{R}^2/\mathbb{Z}^2$ into $(n + 3)^2$ atoms. The encoding of \mathbb{Z}^2 -orbits under R_n by the topological partition \mathcal{P}_n are 2-dimensional configurations whose topological closure is the symbolic dynamical system $\mathcal{X}_{\mathcal{P}_n, R_n}$. The polygonal partition \mathcal{P}_n of the torus can be constructed by drawing the following geodesics on the torus \mathbb{T}^2 :

- a closed geodesic of slope 0 going through the origin $(0, 0)$,
- a closed geodesic of slope 0 going through the point $(0, \beta^{-1})$,
- a geodesic of slope $-\beta^{-1}$ from $(0, \beta^{-1})$ to $(1, 0)$,
- a geodesic of slope $-\beta$ from $(0, \beta^{-1})$ to $(1, 0)$ wrapping around the unit square fundamental domain n times,

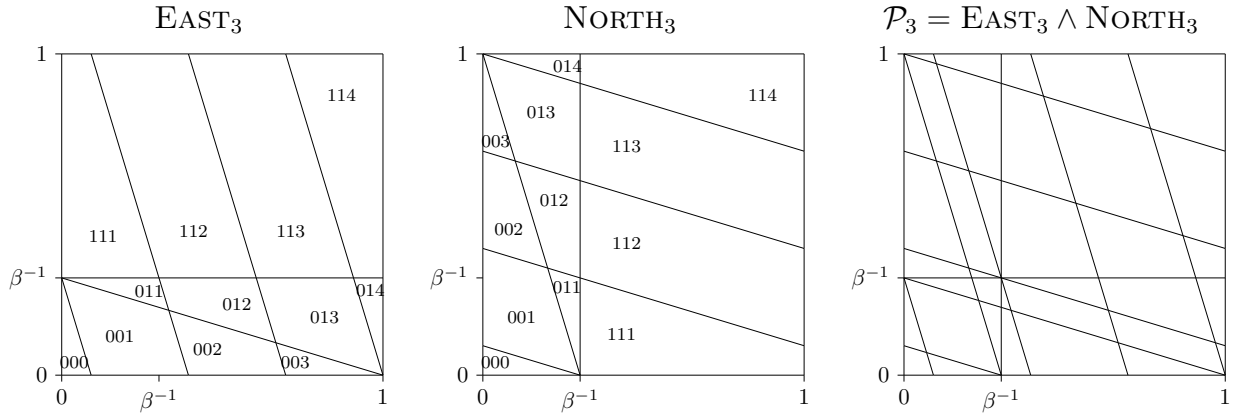


FIGURE 6. The partition EAST_3 and its image NORTH_3 under the positive diagonal. Their refinement is \mathcal{P}_3 which is a partition of the unit square into 36 polygonal atoms. Here β is the third metallic mean, that is, the positive root of $x^2 - 3x - 1$.

together with their symmetric images under the positive diagonal. See an illustration of \mathcal{P}_n when $n = 3$ in Figure 6. Open regions defined by the complement of the geodesics can be identified with pairs of vectors in V_n . See the beginning of Section 9 for more details about the construction of the partition and the symbolic dynamical systems it defines.

We prove that $\mathcal{X}_{\mathcal{P}_n, R_n} = \Omega_n$. Since Ω_n is a subshift of finite type by definition, we have the following theorem.

Theorem F. *For every integer $n \geq 1$, the symbolic dynamical system $\mathcal{X}_{\mathcal{P}_n, R_n}$ corresponding to \mathcal{P}_n, R_n is equal to the metallic mean Wang shift Ω_n :*

$$\mathcal{X}_{\mathcal{P}_n, R_n} = \Omega_n.$$

In particular, \mathcal{P}_n is a Markov partition for the dynamical system $\mathbb{Z}^2 \overset{R_n}{\curvearrowright} \mathbb{T}^2$.

Markov partitions were originally defined for one-dimensional dynamical systems $\mathbb{Z} \overset{T}{\curvearrowright} \mathbb{T}^2$ and were extended to \mathbb{Z}^d -actions by automorphisms of compact Abelian group in [ES97]. Following

[Lab21a,Lab21b], we use the same terminology and extend the definition proposed in [LM95, §6.5] for dynamical systems defined by higher-dimensional actions by rotations, see Definition 9.1.

The Markov partition associated to Jeandel–Rao tiles and action R_0 on \mathbb{R}^2/Γ_0 is related to the golden ratio [Lab21a]. In this contribution, we describe a family of \mathbb{Z}^2 -actions related to the metallic-mean quadratic integers. Can we find examples related to other numbers?

Question 4. *For which \mathbb{Z}^2 -actions defined by rotations on a 2-dimensional torus does there exist a Markov Partition? When is this partition smooth/polygonal?*

As for toral hyperbolic automorphisms, we can expect that smooth Markov partitions are associated to algebraic integers of degree 2 and that the partition is piecewise linear in this case [Caw91]. Markov partitions for typical toral hyperbolic automorphisms have fractal boundaries [Bow78].

The relation with toral hyperbolic automorphisms does not come out of nowhere. Indeed, the self-similarity of Ω_n proved in [Lab23a] has an incidence matrix of size $(n+3)^2 \times (n+3)^2$. Its eigenvalues are all quadratic integers, 0 or ± 1 . This incidence matrix acts hyperbolically as a toral automorphism on a subspace of $\mathbb{R}^{(n+3)^2}$ thus admits a Markov partition with piecewise linear boundaries. A link between this Markov partition and the partition \mathcal{P}_n can be expected, because this is what happens for 1-dimensional sequences. Indeed, the Markov partition associated to the toral automorphism $\begin{pmatrix} 1 & 1 & 1 \\ 1 & 0 & 0 \\ 0 & 1 & 0 \end{pmatrix}$ is a suspension of the Rauzy fractal [Rau82] as nicely illustrated in a talk by Timo Jolivet [Jol12].

Question 5. *What is the relation between the Markov partition for the hyperbolic toral automorphism defined from the incidence matrix of the self-similarity of Ω_n and the Markov partition \mathcal{P}_n associated to $\mathbb{Z}^2 \overset{\sigma}{\curvearrowright} \Omega_n$?*

The symmetric properties of Ω_n and of the partition \mathcal{P}_n make them a good object of study to tackle these questions in more generality.

3. PRELIMINARIES ON DYNAMICAL SYSTEMS, SUBSHIFTS AND WANG SHIFTS

This section follows the preliminary section of the chapter [Lab20] and article [Lab21a].

3.1. Topological dynamical systems. Most of the notions introduced here can be found in [Wal82]. A **dynamical system** is a triple (X, G, T) , where X is a topological space, G is a topological group and T is a continuous function $G \times X \rightarrow X$ defining a left action of G on X : if $x \in X$, e is the identity element of G and $g, h \in G$, then using additive notation for the operation in G we have $T(e, x) = x$ and $T(g + h, x) = T(g, T(h, x))$. In other words, if one denotes the transformation $x \mapsto T(g, x)$ by T^g , then $T^{g+h} = T^g T^h$. In this work, we consider the Abelian group $G = \mathbb{Z} \times \mathbb{Z}$.

If $Y \subset X$, let \overline{Y} denote the topological closure of Y and let $T(Y) := \cup_{g \in G} T^g(Y)$ denote the T -closure of Y . Alternatively, we also use the notation $\overline{Y}^T = T(Y)$ to denote the T -closure of Y . A subset $Y \subset X$ is **T -invariant** if $T(Y) = Y$. A dynamical system (X, G, T) is called **minimal** if X does not contain any nonempty, proper, closed T -invariant subset. The left action of G on X is **free** if $g = e$ whenever there exists $x \in X$ such that $T^g(x) = x$.

Let (X, G, T) and (Y, G, S) be two dynamical systems with the same topological group G . A **homomorphism** $\theta : (X, G, T) \rightarrow (Y, G, S)$ is a continuous function $\theta : X \rightarrow Y$ satisfying the commuting property that $S^g \circ \theta = \theta \circ T^g$ for every $g \in G$. A homomorphism $\theta : (X, G, T) \rightarrow (Y, G, S)$ is called an **embedding** if it is one-to-one, a **factor map** if it is onto, and a **topological conjugacy** if it is both one-to-one and onto and its inverse map is continuous. If $\theta : (X, G, T) \rightarrow (Y, G, S)$ is a factor map, then (Y, G, S) is called a **factor** of (X, G, T) and (X, G, T) is called an **extension** of (Y, G, S) . Two dynamical systems are **topologically conjugate** if there is a topological conjugacy between them.

A **measure-preserving dynamical system** is defined as a system $(X, G, T, \mu, \mathcal{B})$, where μ is a probability measure defined on the Borel σ -algebra \mathcal{B} of subsets of X , and $T^g : X \rightarrow X$ is a measurable map which preserves the measure μ for all $g \in G$, that is, $\mu(T^g(B)) = \mu(B)$ for all $B \in \mathcal{B}$. The measure μ is said to be **T -invariant**. In what follows, when it is clear from the context, we omit the Borel σ -algebra \mathcal{B} of subsets of X and write (X, G, T, μ) to denote a measure-preserving dynamical system.

The set of all T -invariant probability measures of a dynamical system (X, G, T) is denoted by $\mathcal{M}^T(X)$. A T -invariant probability measure on X is called **ergodic** if for every set $B \in \mathcal{B}$ such that $T^g(B) = B$ for all $g \in G$, we have that B has either zero or full measure. A dynamical system (X, G, T) is **uniquely ergodic** if it has only one invariant probability measure, i.e., $|\mathcal{M}^T(X)| = 1$. One can prove that a uniquely ergodic dynamical system is ergodic. A dynamical system (X, G, T) is said **strictly ergodic** if it is uniquely ergodic and minimal.

Let $(X, G, T, \mu, \mathcal{B})$ and $(X', G, T', \mu', \mathcal{B}')$ be two measure-preserving dynamical systems. We say that the two systems are **isomorphic** if there exist measurable sets $X_0 \subset X$ and $X'_0 \subset X'$ of full measure (i.e., $\mu(X \setminus X_0) = 0$ and $\mu'(X' \setminus X'_0) = 0$) with $T^g(X_0) \subset X_0$, $T'^g(X'_0) \subset X'_0$ for all $g \in G$ and there exists a map $\phi : X_0 \rightarrow X'_0$, called an **isomorphism**, that is one-to-one and onto and such that for all $A \in \mathcal{B}'(X'_0)$,

- $\phi^{-1}(A) \in \mathcal{B}(X_0)$,
- $\mu(\phi^{-1}(A)) = \mu'(A)$, and
- $\phi \circ T^g(x) = T'^g \circ \phi(x)$ for all $x \in X_0$ and $g \in G$.

The role of the set X_0 is to make precise the fact that the properties of the isomorphism need to hold only on a set of full measure.

3.2. Maximal equicontinuous factor. A metrizable dynamical system (X, G, T) is called **equicontinuous** if the family of homeomorphisms $\{T^g\}_{g \in G}$ is equicontinuous, i.e., if for all $\varepsilon > 0$ there exists $\delta > 0$ such that

$$\text{dist}(T^g(x), T^g(y)) < \varepsilon$$

for all $g \in G$ and all $x, y \in X$ with $\text{dist}(x, y) < \delta$. According to a well-known theorem [ABKL15, Theorem 3.2], equicontinuous minimal systems defined by the action of an Abelian group are rotations on groups.

We say that $\theta : (X, G, T) \rightarrow (Y, G, S)$ is an **equicontinuous factor** if θ is a factor map and (Y, G, S) is equicontinuous. We say that (X_{\max}, G, T_{\max}) is the **maximal equicontinuous factor** of (X, G, T) if there exists an equicontinuous factor $\pi_{\max} : (X, G, T) \rightarrow (X_{\max}, G, T_{\max})$, such that for any equicontinuous factor $\theta : (X, G, T) \rightarrow (Y, G, S)$, there exists a unique factor map $\psi : (X_{\max}, G, T_{\max}) \rightarrow (Y, G, S)$ with $\psi \circ \pi_{\max} = \theta$. The maximal equicontinuous factor exists and is unique (up to topological conjugacy), see [ABKL15, Theorem 3.8] and [Kur03, Theorem 2.44].

Let $\theta : (X, G, T) \rightarrow (Y, G, S)$ be a factor map. We call the preimage set $\theta^{-1}(y)$ of a point $y \in Y$ the **fiber** of θ over y . The cardinality of the fiber $\theta^{-1}(y)$ for some $y \in Y$ has an important role and is related to the definition of other notions, see [ABKL15]. In particular, the factor map θ is **almost one-to-one** if $\{y \in Y : \text{card}(\theta^{-1}(y)) = 1\}$ is a G_δ -dense set in Y (that is a countable intersection of open sets which is dense in Y). In that case, (X, G, T) is an **almost one-to-one extension** of (Y, G, S) . The **set of fiber cardinalities** of a factor map $\theta : (X, G, T) \rightarrow (Y, G, S)$ is the set $\{\text{card}(\theta^{-1}(y)) : y \in Y\} \subset \mathbb{N} \cup \{\infty\}$, see [Fie01]. The set of fiber cardinalities of the maximal equicontinuous factor of a minimal dynamical system is invariant under topological conjugacy, see for instance [Lab21a, Lemma 2.2].

3.3. Subshifts and shifts of finite type. In this section, we introduce multidimensional subshifts, a particular type of dynamical systems [LM95, §13.10], [Sch01, Lin04, Hoc16]. Let \mathcal{A} be a finite set, $d \geq 1$, and let $\mathcal{A}^{\mathbb{Z}^d}$ be the set of all maps $x : \mathbb{Z}^d \rightarrow \mathcal{A}$, equipped with the compact

product topology. An element $x \in \mathcal{A}^{\mathbb{Z}^d}$ is called **configuration** and we write it as $x = (x_m) = (x_m : m \in \mathbb{Z}^d)$, where $x_m \in \mathcal{A}$ denotes the value of x at m . The topology on $\mathcal{A}^{\mathbb{Z}^d}$ is compatible with the metric defined for all configurations $x, x' \in \mathcal{A}^{\mathbb{Z}^d}$ by $\text{dist}(x, x') = 2^{-\min\{\|\mathbf{n}\| : x_{\mathbf{n}} \neq x'_{\mathbf{n}}\}}$ where $\|\mathbf{n}\| = |n_1| + \dots + |n_d|$. The **shift action** $\sigma : \mathbf{n} \mapsto \sigma^{\mathbf{n}}$ of the additive group \mathbb{Z}^d on $\mathcal{A}^{\mathbb{Z}^d}$ is defined by

$$(3.1) \quad (\sigma^{\mathbf{n}}(x))_m = x_{m+\mathbf{n}}$$

for every $x = (x_m) \in \mathcal{A}^{\mathbb{Z}^d}$ and $\mathbf{n} \in \mathbb{Z}^d$. If $X \subset \mathcal{A}^{\mathbb{Z}^d}$, let \bar{X} denote the topological closure of X and let $\bar{X}^\sigma := \{\sigma^{\mathbf{n}}(x) \mid x \in X, \mathbf{n} \in \mathbb{Z}^d\}$ denote the shift-closure of X . A subset $X \subset \mathcal{A}^{\mathbb{Z}^d}$ is **shift-invariant** if $\bar{X}^\sigma = X$. A closed, shift-invariant subset $X \subset \mathcal{A}^{\mathbb{Z}^d}$ is a **subshift**. If $X \subset \mathcal{A}^{\mathbb{Z}^d}$ is a subshift we write $\sigma = \sigma^X$ for the restriction of the shift action (3.1) to X . When X is a subshift, the triple $(X, \mathbb{Z}^d, \sigma)$ is a dynamical system and the notions presented in the previous section hold.

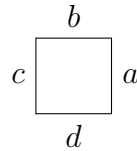
A configuration $x \in X$ is **periodic** if there is a nonzero vector $\mathbf{n} \in \mathbb{Z}^d \setminus \{\mathbf{0}\}$ such that $x = \sigma^{\mathbf{n}}(x)$ and otherwise it is **nonperiodic**. We say that a nonempty subshift X is **aperiodic** if the shift action σ on X is free.

For any subset $S \subset \mathbb{Z}^d$ let $\pi_S : \mathcal{A}^{\mathbb{Z}^d} \rightarrow \mathcal{A}^S$ denote the projection map which restricts every $x \in \mathcal{A}^{\mathbb{Z}^d}$ to S . A **pattern** is a function $p \in \mathcal{A}^S$ for some finite subset $S \subset \mathbb{Z}^d$. To every pattern $p \in \mathcal{A}^S$ corresponds a subset $\pi_S^{-1}(p) \subset \mathcal{A}^{\mathbb{Z}^d}$ called **cylinder**. A nonempty set $X \subset \mathcal{A}^{\mathbb{Z}^d}$ is a **subshift** if and only if there exists a set \mathcal{F} of **forbidden** patterns such that

$$(3.2) \quad X = \{x \in \mathcal{A}^{\mathbb{Z}^d} \mid \pi_S \circ \sigma^{\mathbf{n}}(x) \notin \mathcal{F} \text{ for every } \mathbf{n} \in \mathbb{Z}^d \text{ and } S \subset \mathbb{Z}^d\},$$

see [Hoc16, Prop. 9.2.4]. A subshift $X \subset \mathcal{A}^{\mathbb{Z}^d}$ is a **subshift of finite type** (SFT) if there exists a finite set \mathcal{F} such that (3.2) holds. In this article, we consider shifts of finite type on $\mathbb{Z} \times \mathbb{Z}$, that is, the case $d = 2$.

3.4. Wang shifts. A **Wang tile** is a tuple of four colors $(a, b, c, d) \in I \times J \times I \times J$ where I is a finite set of vertical colors and J is a finite set of horizontal colors, see [Wan61, Rob71]. A Wang tile is represented as a unit square with colored edges:



For each Wang tile $\tau = (a, b, c, d)$, let $\text{RIGHT}(\tau) = a$, $\text{TOP}(\tau) = b$, $\text{LEFT}(\tau) = c$, $\text{BOTTOM}(\tau) = d$ denote respectively the colors of the right, top, left and bottom edges of τ .

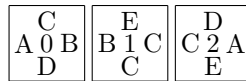


FIGURE 7. The set of 3 Wang tiles introduced in [Wan61] using letters $\{A, B, C, D, E\}$ instead of numbers from the set $\{1, 2, 3, 4, 5\}$ for labeling the edges. Each tile is identified uniquely by an index from the set $\{0, 1, 2\}$ written at the center each tile.

Let $\mathcal{T} = \{t_0, \dots, t_{m-1}\}$ be a set of Wang tiles as the one shown in Figure 7. A configuration $x : \mathbb{Z}^2 \rightarrow \{0, \dots, m-1\}$ is **valid** with respect to \mathcal{T} if it assigns a tile in \mathcal{T} to each position of \mathbb{Z}^2 so that contiguous edges of adjacent tiles have the same color, that is,

$$(3.3) \quad \text{RIGHT}(t_{x(\mathbf{n})}) = \text{LEFT}(t_{x(\mathbf{n}+e_1)})$$

$$(3.4) \quad \text{TOP}(t_{x(\mathbf{n})}) = \text{BOTTOM}(t_{x(\mathbf{n}+e_2)})$$

for every $\mathbf{n} \in \mathbb{Z}^2$ where $\mathbf{e}_1 = (1, 0)$ and $\mathbf{e}_2 = (0, 1)$. A finite pattern which is valid with respect to \mathcal{U} is shown in Figure 8.

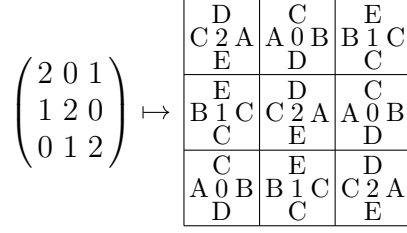


FIGURE 8. A finite 3×3 pattern on the left is valid with respect to the Wang tiles since it respects Equations (3.3) and (3.4). Validity can be verified on the tiling shown on the right.

Let $\Omega_{\mathcal{T}} \subset \{0, \dots, m-1\}^{\mathbb{Z}^2}$ denote the set of all valid configurations with respect to \mathcal{T} , called the **Wang shift** of \mathcal{T} . To a configuration $x \in \Omega_{\mathcal{T}}$ corresponds a tiling of the plane \mathbb{R}^2 by the tiles \mathcal{T} where the unit square Wang tile $t_{x(\mathbf{n})}$ is placed at position \mathbf{n} for every $\mathbf{n} \in \mathbb{Z}^2$, as in Figure 8. Together with the shift action σ of \mathbb{Z}^2 , $\Omega_{\mathcal{T}}$ is a SFT of the form (3.2) since there exists a finite set of forbidden patterns made of all horizontal and vertical dominoes of two tiles that do not share an edge of the same color.

A configuration $x \in \Omega_{\mathcal{T}}$ is **periodic** if there exists $\mathbf{n} \in \mathbb{Z}^2 \setminus \{0\}$ such that $x = \sigma^{\mathbf{n}}(x)$. A set of Wang tiles \mathcal{T} is **periodic** if there exists a periodic configuration $x \in \Omega_{\mathcal{T}}$. Originally, Wang thought that every set of Wang tiles \mathcal{T} is periodic as soon as $\Omega_{\mathcal{T}}$ is nonempty [Wan61]. This statement is equivalent to the existence of an algorithm solving the *domino problem*, that is, taking as input a set of Wang tiles and returning *yes* or *no* whether there exists a valid configuration with these tiles. Berger, a student of Wang, later proved that the domino problem is undecidable and he also provided a first example of an aperiodic set of Wang tiles [Ber66]. A set of Wang tiles \mathcal{T} is **aperiodic** if the Wang shift $\Omega_{\mathcal{T}}$ is a nonempty aperiodic subshift. This means that in general one can not decide the emptiness of a Wang shift $\Omega_{\mathcal{T}}$.

4. THE FAMILY OF METALLIC MEAN WANG TILES

In this section, we recall from [Lab23a] the definition of the set \mathcal{T}_n of metallic mean Wang tiles and the extended set \mathcal{T}'_n which satisfies $\mathcal{T}_n \subset \mathcal{T}'_n$. The extended set \mathcal{T}'_n was used to prove the self-similarity of the Wang shift Ω_n defined over \mathcal{T}'_n .

For every integer $n \in \mathbb{Z}$, we write \bar{n} to denote $n+1$ and \underline{n} to denote $n-1$:

$$\begin{aligned} \bar{n} &:= n+1, \\ \underline{n} &:= n-1. \end{aligned}$$

For every Wang tile $\tau = (a, b, c, d)$, we define its symmetric image under the positive diagonal as $\hat{\tau} = (b, a, d, c)$:

$$\text{if } \tau = \begin{array}{|c|} \hline b \\ \hline c \square a \\ \hline d \\ \hline \end{array}, \quad \text{then} \quad \hat{\tau} = \begin{array}{|c|} \hline a \\ \hline d \square b \\ \hline c \\ \hline \end{array}.$$

4.1. **The tiles.** For every integer $n \geq 1$, let

$$V_n = \{(v_0, v_1, v_2) \in \mathbb{Z}^3 : 0 \leq v_0 \leq v_1 \leq v_2 \leq n + 1 \text{ and } v_1 \leq 1\}.$$

be a set of vectors having non-decreasing entries with an upper bound of 1 on the middle entry and an upper bound of $n + 1$ on the last entry. The label of the edges of the Wang tiles considered in this article are vectors in V_n . To lighten the figures and the presentation of the Wang tiles, it is convenient to denote the vector $(v_0, v_1, v_2) \in V_n$ more compactly as a word $v_0v_1v_2$. For instance the vector $(1, 1, 1)$ is represented as 111 .

To help the reading of the tiles and tilings, we assign a color to the vectors according to the following rule: a vector $v \in 00\mathbb{N}$ is drawn in **blue**, a vector $v \in 01\mathbb{N}$ is drawn in **yellow** and a vector $v \in 11\mathbb{N}$ is drawn in **white**. Overlap between blue and yellow region will be shown in **green**,

For every integer $n \geq 1$ and for every $i, j \in \mathbb{N}$ such that $0 \leq i \leq n$ and $0 \leq j \leq n$, we have the following white tiles:

white tiles	
$w_n^{i,j} =$	

For every $i, n \in \mathbb{N}$ such that $0 \leq i \leq n$, we have the following blue, yellow, green and antigreen tiles:

	horizontal tiles	vertical tiles
blue tiles	$b_n^i =$	$\widehat{b}_n^i =$
yellow tiles	$y_n^i =$	$\widehat{y}_n^i =$
green overlap tiles	$g_n^i =$	$\widehat{g}_n^i =$
antigreen no overlap tiles	$a_n^i =$	$\widehat{a}_n^i =$

For every $n \in \mathbb{N}$ and $k, \ell, r, s \in \{0, 1\}$, we have the following junction tiles (the gray region will be drawn in a blue or yellow color depending on the specific values of k, ℓ, r, s according to the same rule as above):

junction tiles	
$j_n^{k,\ell,r,s} =$	

Junction tiles play a similar role as junction tiles in [Moz89].

4.2. The family \mathcal{T}_n of $(n+3)^2$ Wang tiles. In this section, we give the definition of the family of sets of Wang tiles $(\mathcal{T}_n)_{n \geq 1}$.

From the above, we define the following sets of tiles:

$$\begin{aligned}
 W_n &= \{w_n^{i,j} \mid 1 \leq i \leq n, 1 \leq j \leq n\} && (n^2 \text{ white tiles}), \\
 Y_n &= \{y_n^i \mid 1 \leq i \leq n\} && (n \text{ horizontal yellow tiles}), \\
 G_n &= \{g_n^i \mid 0 \leq i \leq n\} && (n+1 \text{ horizontal green tiles}), \\
 B_n &= \{b_n^i \mid 0 \leq i \leq n-1\} && (n \text{ horizontal blue tiles}), \\
 J_n &= \{j_n^{0,0,0,0}, j_n^{0,1,0,0}, j_n^{0,0,0,1}, j_n^{0,1,0,1}, j_n^{1,1,0,1}, j_n^{0,1,1,1}, j_n^{1,1,1,1}\} && (7 \text{ junction tiles}).
 \end{aligned}$$

Below is an explicit drawing with blue and yellow colors of the 7 junction tiles:

$$J_n = \left(\begin{array}{ccc}
 & \begin{array}{c} 001 \\ \text{01n} \begin{array}{c} \text{011} \\ \text{01}\bar{n} \end{array} \text{011} \\ 01\bar{n} \end{array} & \begin{array}{c} 011 \\ \text{01}\bar{n} \begin{array}{c} \text{011} \\ \text{01}\bar{n} \end{array} \text{011} \\ 01\bar{n} \end{array} \\
 \begin{array}{c} 000 \\ \text{00n} \begin{array}{c} \text{001} \\ \text{01n} \end{array} \text{001} \\ 01n \end{array} & \begin{array}{c} 001 \\ \text{01n} \begin{array}{c} \text{001} \\ \text{01n} \end{array} \text{001} \\ 01n \end{array} & \begin{array}{c} 011 \\ \text{01}\bar{n} \begin{array}{c} \text{011} \\ \text{01n} \end{array} \text{001} \\ 01n \end{array} \\
 \begin{array}{c} 000 \\ \text{00n} \begin{array}{c} \text{001} \\ \text{00n} \end{array} \text{000} \\ 00n \end{array} & \begin{array}{c} 001 \\ \text{01n} \begin{array}{c} \text{001} \\ \text{00n} \end{array} \text{000} \\ 00n \end{array} &
 \end{array} \right)$$

We may observe that $\widehat{W}_n = W_n$ and $\widehat{J}_n = J_n$. Also, \widehat{Y}_n are n vertical yellow tiles, \widehat{G}_n are $n+1$ vertical green tiles and \widehat{B}_n are n vertical blue tiles.

Definition 4.1 (Metallic Mean Wang tiles). *For every positive integer n , we construct the set of Wang tiles*

$$\mathcal{T}_n = W_n \cup Y_n \cup \widehat{Y}_n \cup G_n \cup \widehat{G}_n \cup B_n \cup \widehat{B}_n \cup J_n.$$

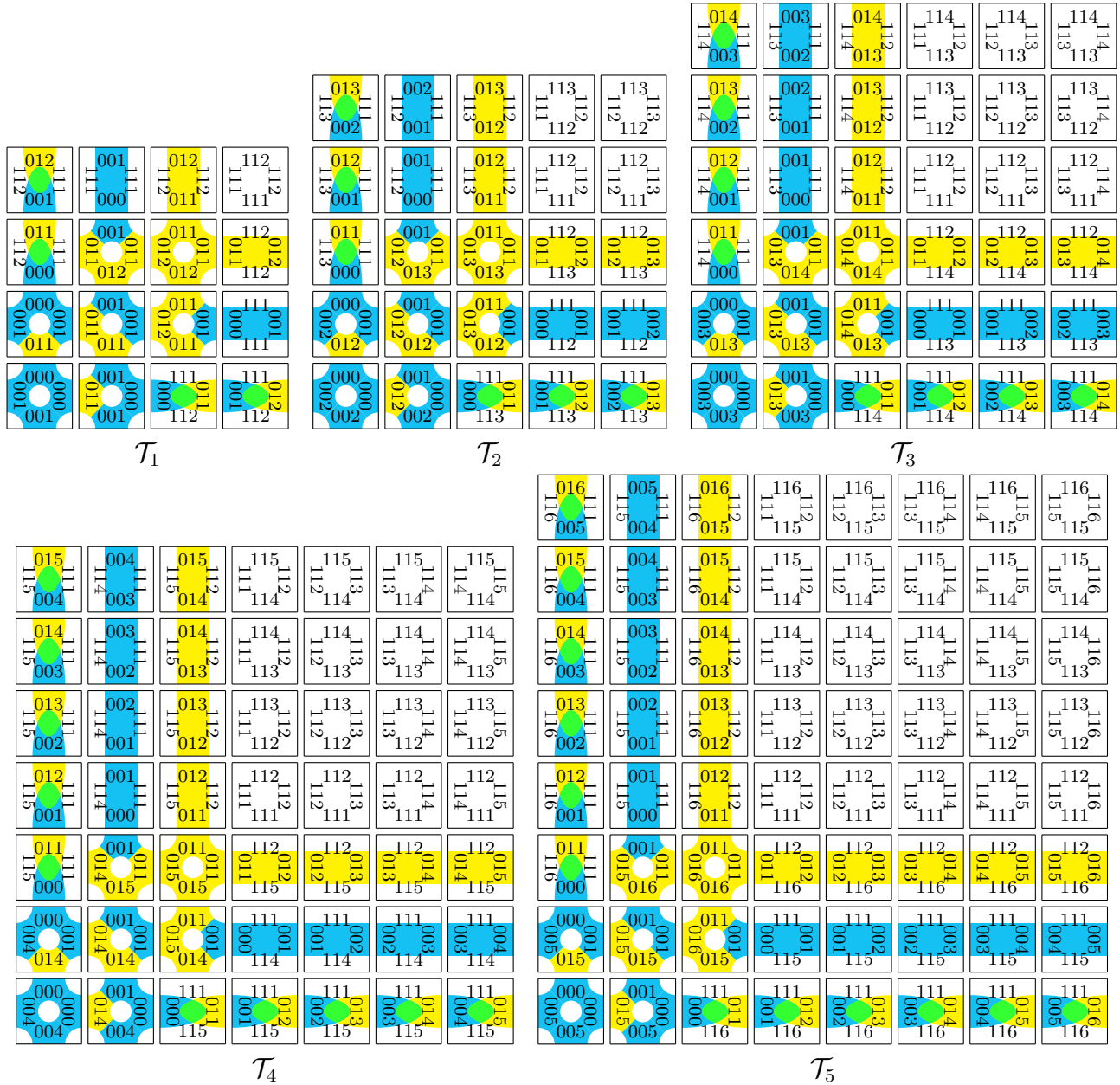
The set of tiles defines the **Metallic mean Wang shift** $\Omega_n = \Omega_{\mathcal{T}_n}$.

The set \mathcal{T}_n contains $n^2 + 2n + 2(n+1) + 2n + 7 = (n+3)^2$ Wang tiles. It is shown in Figure 9 for $n = 1, 2, 3, 4, 5$. A typical part of a valid tiling is shown in Figure 10 over the set \mathcal{T}_3 . More images of valid tilings with metallic mean Wang tiles are available in [Lab23a].

4.3. A larger set \mathcal{T}'_n of Wang tiles. In order to describe the structure of the Wang shift Ω_n generated from the set \mathcal{T}_n , we need to introduce a larger set \mathcal{T}'_n satisfying $\mathcal{T}_n \subseteq \mathcal{T}'_n$. The set \mathcal{T}'_n can be described in terms of the white, yellow, green, blue, antigreen and junction tiles seen before.

Definition 4.2. *Let*

$$\mathcal{T}'_n = W_n \cup Y_n \cup \widehat{Y}_n \cup G_n \cup \widehat{G}_n \cup B'_n \cup \widehat{B}'_n \cup A_n \cup \widehat{A}_n \cup J'_n$$

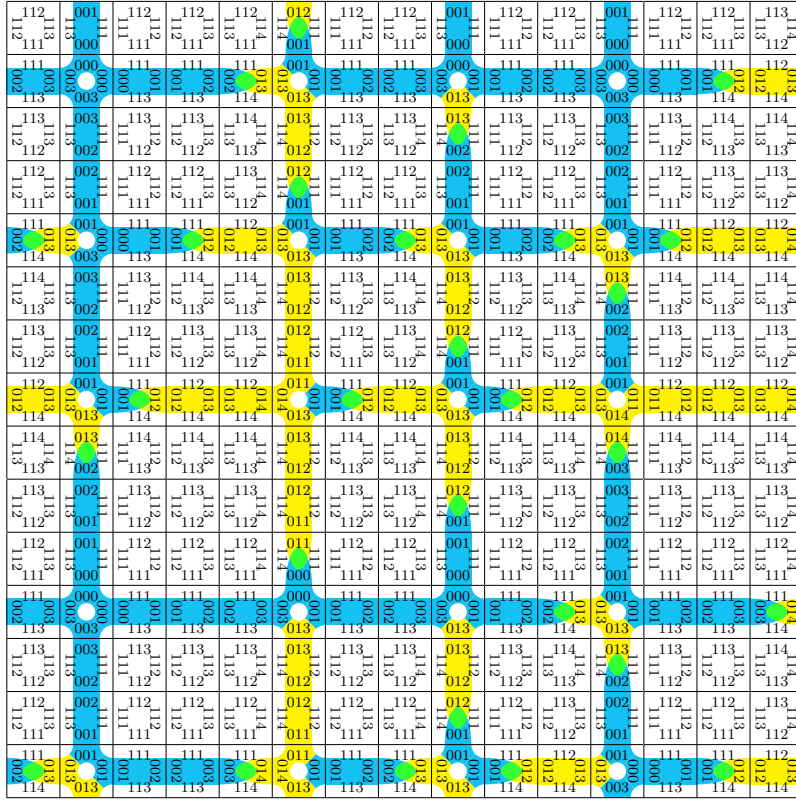
FIGURE 9. Metallic mean Wang tile sets \mathcal{T}_n for $n = 1, 2, 3, 4, 5$.

where

$$\begin{aligned}
 B'_n &= B_n \cup \{b_n^n\} && \text{(extended set of } n+1 \text{ horizontal blue tiles),} \\
 J'_n &= J_n \cup \{j_n^{1,1,0,0}, j_n^{0,0,1,1}\} && \text{(extended set of 9 junction tiles),} \\
 A_n &= \{a_n^i \mid 1 \leq i \leq n\} && \text{(} n \text{ antigreen tiles).}
 \end{aligned}$$

The set of tiles defines the **extended metallic mean Wang shift** $\Omega'_n = \Omega_{\mathcal{T}'_n}$.

The set \mathcal{T}'_n contains $(n+3)^2 + 2 + 2n + 2 = n^2 + 8n + 13$ Wang tiles. In particular, the set \mathcal{T}'_n contains the tiles from the set \mathcal{T}_n . The set of Wang tiles \mathcal{T}'_n for $n = 4$ is shown in Figure 11.


 FIGURE 10. A valid 15×15 pattern with Wang tile set \mathcal{T}_3 .

5. THE θ_n -CHIP AND METALLIC MEAN WANG TILES

Recall that \mathcal{C}_n is the set of Wang tiles defined from the instances of the θ_n -chip, see Equation 2.2.

Proposition 5.1. *We have*

$$\mathcal{C}_n = \mathcal{T}'_n$$

where \mathcal{T}'_n is the extended set of metallic mean Wang tiles introduced in [Lab23a].

$$\theta_n(v, u)$$

Proof. (\subseteq) Let $\tau = \begin{array}{c} u \begin{array}{|c|} \hline \square \\ \hline \end{array} \theta_n(u, v) \\ v \end{array}$ be a Wang tile such that $u = (u_0, u_1, u_2) \in V_n$, $v =$

$(v_0, v_1, v_2) \in V_n$, $\theta_n(u, v) \in V_n$ and $\theta_n(v, u) \in V_n$. We proceed case by case:

- If $u_0 = 1$ and $v_0 = 1$, then $1 = u_1 \leq u_2$, $1 = v_1 \leq v_2$ and

$$\theta_n(u, v) = (u_0, 1, u_2 + 1) = (1, 1, u_2 + 1) \in V_n,$$

$$\theta_n(v, u) = (v_0, 1, v_2 + 1) = (1, 1, v_2 + 1) \in V_n.$$

Thus $0 \leq u_2 \leq n$ and $0 \leq v_2 \leq n$ and $\tau \in W_n$ is a white tile.

- If $u_0 = 0$ and $v_0 = 1$, then

$$\theta_n(u, v) = (u_0, v_2 - n, u_2 + 1) = (0, v_2 - n, u_2 + 1) \in V_n,$$

$$\theta_n(v, u) = (v_0, 1, u_1 + v_0) = (1, 1, u_1 + 1) \in V_n,$$

where $0 \leq u_2 \leq n$, $n \leq v_2 \leq n + 1$ and $0 \leq u_1 \leq 1$.

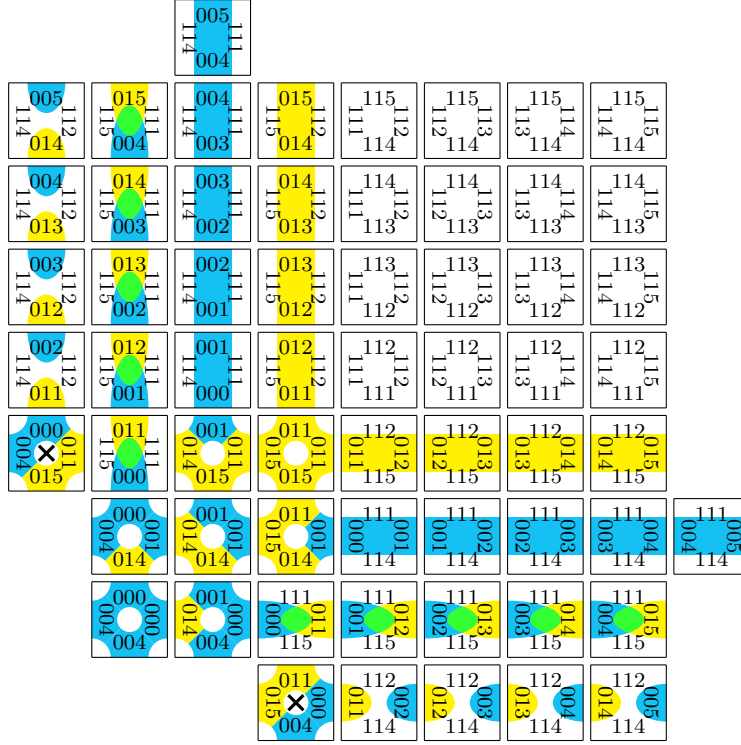


FIGURE 11. Extended metallic mean Wang tile sets \mathcal{T}'_n for $n = 4$. The junction tiles $j_n^{0,0,1,1}$ and $j_n^{1,1,0,0}$ are shown with a \times -mark in their center.

- If $v_2 = n$ and $u_1 = 0$, then $\tau = \begin{matrix} (1, 1, 1) \\ (0, 0, u_2) \square (0, 0, u_2 + 1) \\ (1, 1, n) \end{matrix} = b_n^{u_2} \in B_n \cup \{b_n^n\}$ is a blue horizontal stripe tile with $0 \leq u_2 \leq n$.
- If $v_2 = n$ and $u_1 = 1$, then $\tau = \begin{matrix} (1, 1, 2) \\ (0, 1, u_2) \square (0, 0, u_2 + 1) \\ (1, 1, n) \end{matrix} = a_n^{u_2} \in A_n$ is an antigreen horizontal tile with $1 \leq u_2 \leq n$.
- If $v_2 = n + 1$ and $u_1 = 0$, then $\tau = \begin{matrix} (1, 1, 1) \\ (0, 0, u_2) \square (0, 1, u_2 + 1) \\ (1, 1, n + 1) \end{matrix} = g_n^{u_2} \in G_n$ is a green horizontal overlap tile with $0 \leq u_2 \leq n$.
- If $v_2 = n + 1$ and $u_1 = 1$, then $\tau = \begin{matrix} (1, 1, 2) \\ (0, 1, u_2) \square (0, 1, u_2 + 1) \\ (1, 1, n + 1) \end{matrix} = y_n^{u_2} \in Y_n$ is a yellow horizontal stripe tile with $1 \leq u_2 \leq n$.

- If $u_0 = 1$ and $v_0 = 0$, the possibilities are the symmetric image of the previous case. Thus $\tau \in \widehat{B}_n \cup \{\widehat{b}_n^n\} \cup \widehat{A}_n \cup \widehat{G}_n \cup \widehat{Y}_n$ is a blue, antigreen, green or yellow vertical tile.
- If $u_0 = 0$ and $v_0 = 0$, then

$$\begin{aligned}\theta_n(u, v) &= (u_0, v_2 - n, v_1 + u_0) = (0, v_2 - n, v_1) \in V_n, \\ \theta_n(v, u) &= (v_0, u_2 - n, u_1 + v_0) = (0, u_2 - n, u_1) \in V_n,\end{aligned}$$

where $0 \leq u_2 - n \leq u_1 \leq 1$ and $0 \leq v_2 - n \leq v_1 \leq 1$. In particular, $(v_2 - n, v_1), (u_2 - n, u_1) \in \{(0, 0), (0, 1), (1, 1)\}$. In all cases, we have $\tau =$

$$(0, u_1, u_2) \begin{array}{|c|} \hline \square \\ \hline \end{array} \begin{array}{l} (0, v_2 - n, v_1) \\ (0, v_1, v_2) \end{array} \in J_n \cup \{j_n^{0,0,1,1}, j_n^{1,1,0,0}\}$$

is a junction tile.

$$(\supseteq) \text{ Reciprocally, for every } \tau = \ell \begin{array}{|c|} \hline t \\ \hline \square \\ \hline b \\ \hline \end{array} r \in \mathcal{T}'_n, \text{ we observe that } r, t, \ell, b \in V_n, r = \theta_n(\ell, b)$$

and $t = \theta_n(b, \ell)$. □

Observe that \mathcal{T}'_n is obtained in [Lab23a] from the description of the return blocks in configurations of Ω_n . Therefore Proposition 5.1 provides an independent characterization of the set \mathcal{T}'_n as instances of the θ_n -chip.

Theorem A. *For every integer $n \geq 1$, the Wang shift $\Omega_{\mathcal{C}_n}$ defined by the θ_n -chip is the n^{th} metallic mean Wang shift Ω_n .*

Proof. From Proposition 5.1, we have $\mathcal{C}_n = \mathcal{T}'_n$. In [Lab23a], a subset $\mathcal{T}_n \subset \mathcal{T}'_n$ of $(n+3)^2$ Wang tiles was introduced. It was shown that the tiles in the difference set $\mathcal{T}'_n \setminus \mathcal{T}_n$ do not appear in valid configurations of $\Omega_{\mathcal{T}'_n}$. Thus $\Omega_{\mathcal{T}'_n} = \Omega_{\mathcal{T}_n}$. Thus, we conclude the equalities

$$\Omega_{\mathcal{C}_n} = \Omega_{\mathcal{T}'_n} = \Omega_{\mathcal{T}_n} = \Omega_n. \quad \square$$

Now, we show that the computation performed by θ_n is invertible. Let

$$\psi_n : \begin{array}{ccc} V_n \times V_n & \rightarrow & \mathbb{Z}^3 \\ (r_0, r_1, r_2), (t_0, t_1, t_2) & \mapsto & (\ell_0, \ell_1, \ell_2), \end{array}$$

be the function defined by

$$(5.1) \quad \left\{ \begin{array}{l} \ell_0 = r_0, \\ \ell_1 = \begin{cases} t_2 - t_0 & \text{if } r_0 = 0, \\ 1 & \text{if } r_0 = 1, \end{cases} \\ \ell_2 = \begin{cases} t_1 + n & \text{if } t_0 = 0, \\ r_2 - 1 & \text{if } t_0 = 1. \end{cases} \end{array} \right.$$

The following proposition states that the south and west colors can be deduced from the right and top colors.

Proposition 5.2. *We have*

$$(5.2) \quad \mathcal{C}_n = \left\{ \begin{array}{c} \psi_n(r, t) \begin{array}{|c|} \hline t \\ \hline \square \\ \hline \psi_n(t, r) \\ \hline \end{array} r \\ \left| r, t \in V_n \text{ such that } \psi_n(r, t), \psi_n(t, r) \in V_n \right. \end{array} \right\}.$$

Proof. Let $\ell, b \in V_n$ and suppose that $r = (r_0, r_1, r_2) = \theta_n(\ell, b)$ and $t = (t_0, t_1, t_2) = \theta_n(b, \ell)$. From Equation (5.1), we have

$$(5.3) \quad \left\{ \begin{array}{l} r_0 = \ell_0, \\ r_1 = \begin{cases} b_2 - n & \text{if } \ell_0 = 0, \\ 1 & \text{if } \ell_0 = 1, \end{cases} \\ r_2 = \begin{cases} b_1 + \ell_0 & \text{if } b_0 = 0, \\ \ell_2 + 1 & \text{if } b_0 = 1, \end{cases} \end{array} \right. \quad \text{and} \quad \left\{ \begin{array}{l} t_0 = b_0, \\ t_1 = \begin{cases} \ell_2 - n & \text{if } b_0 = 0, \\ 1 & \text{if } b_0 = 1, \end{cases} \\ t_2 = \begin{cases} \ell_1 + b_0 & \text{if } \ell_0 = 0, \\ b_2 + 1 & \text{if } \ell_0 = 1. \end{cases} \end{array} \right.$$

The above holds if and only if

$$\left\{ \begin{array}{l} \ell_0 = r_0, \\ \ell_1 = \begin{cases} t_2 - t_0 & \text{if } r_0 = 0, \\ 1 & \text{if } r_0 = 1, \end{cases} \\ \ell_2 = \begin{cases} t_1 + n & \text{if } t_0 = 0, \\ r_2 - 1 & \text{if } t_0 = 1, \end{cases} \end{array} \right. \quad \text{and} \quad \left\{ \begin{array}{l} b_0 = t_0, \\ b_1 = \begin{cases} r_2 - r_0 & \text{if } t_0 = 0, \\ 1 & \text{if } t_0 = 1, \end{cases} \\ b_2 = \begin{cases} r_1 + n & \text{if } r_0 = 0, \\ t_2 - 1 & \text{if } r_0 = 1. \end{cases} \end{array} \right.$$

if and only if $\ell = (\ell_0, \ell_1, \ell_2) = \psi_n(r, t)$ and $b = (b_0, b_1, b_2) = \psi_n(t, r)$. Thus, from Equation (2.2), we have

$$\begin{aligned} \mathcal{C}_n &= \left\{ \begin{array}{c} \theta_n(b, \ell) \\ \ell \begin{array}{|c|} \hline \square \\ \hline b \\ \hline \end{array} \theta_n(\ell, b) \\ \left| \ell, b \in V_n \text{ such that } \theta_n(\ell, b), \theta_n(b, \ell) \in V_n \right. \end{array} \right\} \\ &= \left\{ \begin{array}{c} \psi_n(r, t) \begin{array}{|c|} \hline t \\ \hline \square \\ \hline \psi_n(t, r) \\ \hline \end{array} r \\ \left| r, t \in V_n \text{ such that } \psi_n(r, t), \psi_n(t, r) \in V_n \right. \end{array} \right\}. \quad \square \end{aligned}$$

As a consequence of Proposition 5.1 and Proposition 5.2, there is a bijection between the south-west and the north-east colors for the tiles in \mathcal{C}_n . Using the vocabulary of [KP99], the set of Wang tile \mathcal{C}_n is North-East-deterministic by definition and South-West deterministic from Proposition 5.2.

6. EQUATIONS SATISFIED BY THE WANG TILES AND THEIR TILINGS

In this section, we show that the set \mathcal{C}_n of Wang tiles satisfy a system of equations. Moreover, we show that the rectangular tilings (of shapes $h \times 1$, $\infty \times 1$ and $h \times k$) generated by them satisfy equations. While the equations associated with Kari's [Kar96] and Culik's [Cul96] aperiodic sets of Wang tiles are multiplicative, the ones associated with \mathcal{C}_n are additive.

In the next theorem, we show that tiles in \mathcal{C}_n satisfy equations which reminds of Equation (1.1).

Theorem B. *Let $n \geq 1$ be an integer, $d = (0, -1, 1)$ and $e = (1, 0, 0)$. The set of Wang tiles defined by the θ_n -chip satisfy the following system of equations:*

$$\mathcal{C}_n \subseteq \left\{ \begin{array}{c} \begin{array}{c} t \\ \square \\ \ell \quad \square \quad r \\ \square \\ b \end{array} \in V_n \times V_n \times V_n \times V_n \quad \left| \quad \begin{array}{l} \langle \frac{1}{n}d, t + \ell \rangle = \langle \frac{1}{n}d, b + r \rangle + \langle e, \ell - b \rangle \\ \langle e, \ell \rangle = \langle e, r \rangle \\ \langle e, b \rangle = \langle e, t \rangle \end{array} \right. \end{array} \right\}$$

where $\langle _, _ \rangle$ denotes the canonical inner product of \mathbb{Z}^3 .

Proof. Let $\ell = (\ell_0, \ell_1, \ell_2)$, $b = (b_0, b_1, b_2)$, $r = (r_0, r_1, r_2)$ and $t = (t_0, t_1, t_2)$. We always have $r_0 = \ell_0$ and $t_0 = b_0$. Thus $\langle e, \ell \rangle = \ell_0 = r_0 = \langle e, r \rangle$ and $\langle e, b \rangle = b_0 = t_0 = \langle e, t \rangle$. Moreover,

$$\begin{aligned} \langle d, b \rangle &= b_2 - b_1, \\ \langle d, \ell \rangle &= \ell_2 - \ell_1. \end{aligned}$$

The proof of the remaining equality is split in four cases. We use Equation (5.3) in the computations below.

- If $(b_0, \ell_0) = (0, 0)$, then

$$\begin{aligned} \langle d, t + \ell \rangle &= (t_2 - t_1) + (\ell_2 - \ell_1) = (\ell_1 + b_0) - (\ell_2 - n) + (\ell_2 - \ell_1) = b_0 + n = n \\ \langle d, r + b \rangle &= (r_2 - r_1) + (b_2 - b_1) = (b_1 + \ell_0) - (b_2 - n) + (b_2 - b_1) = \ell_0 + n = n \\ n\langle e, \ell - b \rangle &= n(\ell_0 - b_0) = 0 \end{aligned}$$

- If $(b_0, \ell_0) = (0, 1)$, then $\ell_1 = 1$ and

$$\begin{aligned} \langle d, t + \ell \rangle &= (t_2 - t_1) + (\ell_2 - \ell_1) = (b_2 + 1) - (\ell_2 - n) + (\ell_2 - \ell_1) = b_2 + n \\ \langle d, r + b \rangle &= (r_2 - r_1) + (b_2 - b_1) = (b_1 + \ell_0) - (1) + (b_2 - b_1) = b_2 \\ n\langle e, \ell - b \rangle &= n(\ell_0 - b_0) = n \end{aligned}$$

- If $(b_0, \ell_0) = (1, 0)$, then $b_1 = 1$ and

$$\begin{aligned} \langle d, t + \ell \rangle &= (t_2 - t_1) + (\ell_2 - \ell_1) = (\ell_1 + b_0) - (1) + (\ell_2 - \ell_1) = \ell_2 \\ \langle d, r + b \rangle &= (r_2 - r_1) + (b_2 - b_1) = (\ell_2 + 1) - (b_2 - n) + (b_2 - b_1) = \ell_2 + n \\ n\langle e, \ell - b \rangle &= n(\ell_0 - b_0) = -n \end{aligned}$$

- If $(b_0, \ell_0) = (1, 1)$, then $b_1 = \ell_1 = 1$ and

$$\begin{aligned} \langle d, t + \ell \rangle &= (t_2 - t_1) + (\ell_2 - \ell_1) = (b_2 + 1) - (1) + (\ell_2 - \ell_1) = b_2 + \ell_2 - \ell_1 \\ \langle d, r + b \rangle &= (r_2 - r_1) + (b_2 - b_1) = (\ell_2 + 1) - (1) + (b_2 - b_1) = \ell_2 + b_2 - b_1 \\ n\langle e, \ell - b \rangle &= n(\ell_0 - b_0) = 0 \end{aligned}$$

In all the four cases, we have $\langle d, t + \ell \rangle = \langle d, r + b \rangle + n\langle e, \ell - b \rangle$. □

Equation (1.1) behaves well with valid tiling of an horizontal strip by Wang tiles associated with the same multiplication factor $q \in \mathbb{Q}$. The same holds with tiles in \mathcal{C}_n which are related to some addition of a certain value modulo 1.

The equation satisfied by the tiles proved in Theorem B extends to an equation for $h \times k$ rectangular valid tilings.

Lemma 6.1. *Let $n, h, k \geq 1$ be integers and $d = (0, -1, 1)$ and $e = (1, 0, 0)$. Let*

$$\{(r^{(i,j)}, t^{(i,j)}, \ell^{(i,j)}, b^{(i,j)})\}_{1 \leq i \leq h, 1 \leq j \leq k}$$

$$T = \frac{1}{h} \sum_{i=1}^h t^{(i,k)}$$

$t^{(1,k)}$	$t^{(2,k)}$	$t^{(3,k)}$...	$t^{(h,k)}$
$\ell^{(1,k)}$	$\ell^{(2,k)}$	$\ell^{(3,k)}$...	$\ell^{(h,k)}$
$b^{(1,k)}$	$b^{(2,k)}$	$b^{(3,k)}$...	$b^{(h,k)}$
⋮	⋮	⋮		⋮

$$L = \frac{1}{k} \sum_{j=1}^k \ell^{(1,j)}$$

$t^{(1,3)}$	$t^{(2,3)}$	$t^{(3,3)}$...	$t^{(h,3)}$
$\ell^{(1,3)}$	$\ell^{(2,3)}$	$\ell^{(3,3)}$...	$\ell^{(h,3)}$
$b^{(1,3)}$	$b^{(2,3)}$	$b^{(3,3)}$...	$b^{(h,3)}$
$t^{(1,2)}$	$t^{(2,2)}$	$t^{(3,2)}$...	$t^{(h,2)}$
$\ell^{(1,2)}$	$\ell^{(2,2)}$	$\ell^{(3,2)}$...	$\ell^{(h,2)}$
$b^{(1,2)}$	$b^{(2,2)}$	$b^{(3,2)}$...	$b^{(h,2)}$
$t^{(1,1)}$	$t^{(2,1)}$	$t^{(3,1)}$...	$t^{(h,1)}$
$\ell^{(1,1)}$	$\ell^{(2,1)}$	$\ell^{(3,1)}$...	$\ell^{(h,1)}$
$b^{(1,1)}$	$b^{(2,1)}$	$b^{(3,1)}$...	$b^{(h,1)}$

$$R = \frac{1}{k} \sum_{j=1}^k r^{(h,j)}$$

$$B = \frac{1}{h} \sum_{i=1}^h b^{(i,1)}$$

FIGURE 12. A $h \times k$ rectangular tiling of tiles from \mathcal{C}_n .

be a family of tiles in \mathcal{C}_n forming a valid tiling of a $h \times k$ rectangle, see Figure 12. Let

$$R = \frac{1}{k} \sum_{j=1}^k r^{(h,j)}, \quad T = \frac{1}{h} \sum_{i=1}^h t^{(i,k)}, \quad L = \frac{1}{k} \sum_{j=1}^k \ell^{(1,j)} \quad \text{and} \quad B = \frac{1}{h} \sum_{i=1}^h b^{(i,1)}$$

be the average of the right, top, left and bottom labels of the rectangular tiling. Then the following equation holds

$$(6.1) \quad \frac{1}{k} \left\langle \frac{1}{n}d, T - B \right\rangle - \langle e, L \rangle = \frac{1}{h} \left\langle \frac{1}{n}d, R - L \right\rangle - \langle e, B \rangle.$$

Proof. From Theorem B, we have $\langle e, \ell^{(i,j)} \rangle = \langle e, r^{(i,j)} \rangle$, $\langle e, b^{(i,j)} \rangle = \langle e, t^{(i,j)} \rangle$ and

$$\left\langle \frac{1}{n}d, t^{(i,j)} - b^{(i,j)} \right\rangle - \langle e, \ell^{(i,j)} \rangle = \left\langle \frac{1}{n}d, r^{(i,j)} - \ell^{(i,j)} \right\rangle - \langle e, b^{(i,j)} \rangle,$$

for every integers i and j such that $1 \leq i \leq h$ and $1 \leq j \leq k$. We have

$$\begin{aligned} \frac{1}{k} \left\langle \frac{1}{n}d, T - B \right\rangle - \langle e, L \rangle &= \frac{1}{k} \left\langle \frac{1}{n}d, \frac{1}{h} \sum_{i=1}^h t^{(i,k)} - \frac{1}{h} \sum_{i=1}^h b^{(i,1)} \right\rangle - \langle e, \frac{1}{k} \sum_{j=1}^k \ell^{(1,j)} \rangle \\ &= \frac{1}{kh} \sum_{i=1}^h \left\langle \frac{1}{n}d, t^{(i,k)} - b^{(i,1)} \right\rangle - \frac{1}{k} \sum_{j=1}^k \langle e, \ell^{(1,j)} \rangle \\ &= \frac{1}{kh} \sum_{i=1}^h \left\langle \frac{1}{n}d, \sum_{j=1}^k t^{(i,j)} - \sum_{j=1}^k b^{(i,j)} \right\rangle - \frac{1}{k} \sum_{j=1}^k \langle e, \frac{1}{h} \sum_{i=1}^h \ell^{(i,j)} \rangle \end{aligned}$$

$$\begin{aligned}
&= \frac{1}{kh} \sum_{i=1}^h \sum_{j=1}^k \left(\left\langle \frac{1}{n}d, t^{(i,j)} - b^{(i,j)} \right\rangle - \langle e, \ell^{(i,j)} \rangle \right) \\
&= \frac{1}{kh} \sum_{i=1}^h \sum_{j=1}^k \left(\left\langle \frac{1}{n}d, r^{(i,j)} - \ell^{(i,j)} \right\rangle - \langle e, b^{(i,j)} \rangle \right) \\
&= \frac{1}{kh} \sum_{j=1}^k \left\langle \frac{1}{n}d, \sum_{i=1}^h r^{(i,j)} - \sum_{i=1}^h \ell^{(i,j)} \right\rangle - \frac{1}{h} \sum_{i=1}^h \left\langle e, \frac{1}{k} \sum_{j=1}^k b^{(i,j)} \right\rangle \\
&= \frac{1}{kh} \sum_{j=1}^k \left\langle \frac{1}{n}d, r^{(h,j)} - \ell^{(1,j)} \right\rangle - \frac{1}{h} \sum_{i=1}^h \langle e, b^{(i,1)} \rangle \\
&= \frac{1}{h} \left\langle \frac{1}{n}d, \frac{1}{k} \sum_{j=1}^k r^{(h,j)} - \frac{1}{k} \sum_{j=1}^k \ell^{(1,j)} \right\rangle - \left\langle e, \frac{1}{h} \sum_{i=1}^h b^{(i,1)} \right\rangle \\
&= \frac{1}{h} \left\langle \frac{1}{n}d, R - L \right\rangle - \langle e, B \rangle. \quad \square
\end{aligned}$$

Equation (6.1) is a simple consequence of the equations satisfied by the tiles, but it has important implications. If $L = R$, then $\left\langle \frac{1}{n}d, R - L \right\rangle = 0$ and $k\langle e, L \rangle$ is an integer. Thus the average of the inner product with $\frac{1}{n}d$ of the top labels is obtained from the average of the inner product with $\frac{1}{n}d$ of the below labels by k rotations on the unit circle by a fixed angle:

$$(6.2) \quad \left\langle \frac{1}{n}d, T \right\rangle = \left\langle \frac{1}{n}d, B \right\rangle - k\langle e, B \rangle \pmod{1}.$$

If Ω_n admits a periodic tiling, then there exists a $h \times k$ rectangular tiling of tiles from \mathcal{C}_n such that $L = R$ and $B = T$. From Equation (6.1), we get that $\langle e, L \rangle = \langle e, B \rangle$. This equation means that the number of rows with no junction tiles is equal to the number of columns with no junction tiles, but this is not sufficient to prove that no periodic tiling exist.

Kari's [Kar96] and Culik's [Cul96] equations allow to show in few lines that their sets of Wang tiles admit no periodic tiling. Proving the same for Ω_n directly from the equations remains an open question.

7. VALID TILINGS OBTAINED FROM FLOORS OF LINEAR FORMS

In this section, we present a method to construct valid tilings in Ω_n . It is based on the integer-floor value of three specific linear form over two variables.

Let $n \geq 1$ be an integer and let β be the positive root of $x^2 - nx - 1$. We denote the negative root by β^* which satisfies $\beta\beta^* = -1$ and $\beta + \beta^* = n$. We consider the matrix

$$M_n = \begin{pmatrix} 0 & 1 \\ \beta^{-1} & 1 \\ \beta & 1 \end{pmatrix}$$

and the map $\lambda_n : \mathbb{R}^2 \rightarrow \mathbb{R}^3$ defined by

$$\lambda_n(x, y) = M_n \cdot \begin{pmatrix} \{x\} \\ \{y\} \end{pmatrix} + \begin{pmatrix} \beta^* + 1 \\ \beta^* + 1 \\ \beta^* + 1 \end{pmatrix}$$

where $\{x\} = x - \lfloor x \rfloor$ is the fractional part of x . Since $\lambda_n(x, y) = \lambda_n(x + 1, y) = \lambda_n(x, y + 1)$, it is also well-defined on the torus $\lambda_n : \mathbb{T}^2 \rightarrow \mathbb{R}^3$. Then, we define a coding function Λ_n as the

coordinate-wise floor of λ_n when restricted to the domain $[0, 1]^2$. More precisely, we have

$$\Lambda_n : [0, 1]^2 \rightarrow \mathbb{Z}^3$$

$$(x, y) \mapsto \begin{pmatrix} \lfloor y + \beta^* + 1 \rfloor \\ \lfloor \beta^{-1}x + y + \beta^* + 1 \rfloor \\ \lfloor \beta x + y + \beta^* + 1 \rfloor \end{pmatrix},$$

see Figure 13.

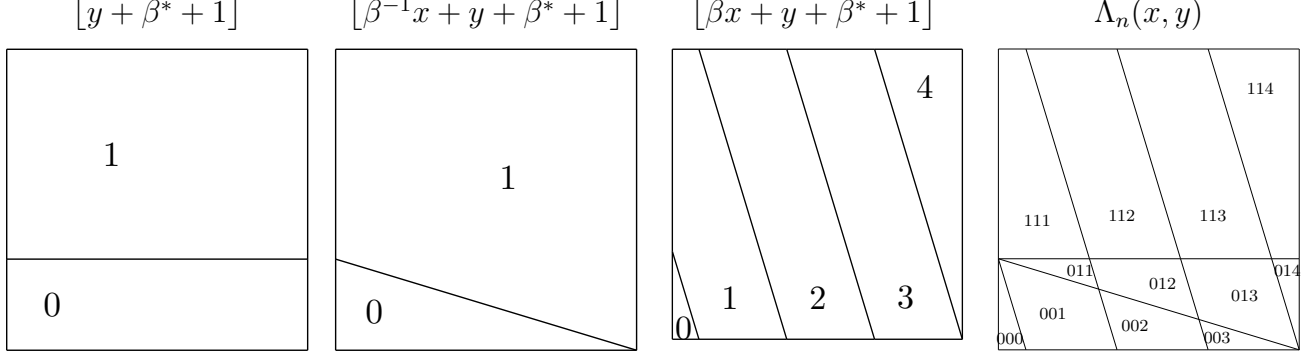


FIGURE 13. The preimage sets of the map $(x, y) \mapsto \Lambda_n(x, y)$ defines a partition of $[0, 1]^2$ which is the refinement of the three partitions on the left. The above images are when $n = 3$.

Recall that, for every integer $n \geq 1$, we have

$$V_n = \{(v_0, v_1, v_2) \in \mathbb{Z}^3 : 0 \leq v_0 \leq v_1 \leq v_2 \leq n + 1 \text{ and } v_1 \leq 1\}.$$

Lemma 7.1. *For every $(x, y) \in [0, 1]^2$, $\Lambda_n(x, y) \in V_n$.*

Proof. Let $(x, y) \in [0, 1]^2$. Since $\beta > 1$, we have

$$0 < \beta^* + 1 \leq y + \beta^* + 1 \leq \beta^{-1}x + y + \beta^* + 1 \leq \beta x + y + \beta^* + 1 < \beta + 1 + \beta^* + 1 = n + 2.$$

Thus, taking the floor function, we obtain

$$0 \leq \lfloor \beta^* + 1 \rfloor \leq \lfloor y + \beta^* + 1 \rfloor \leq \lfloor \beta^{-1}x + y + \beta^* + 1 \rfloor \leq \lfloor \beta x + y + \beta^* + 1 \rfloor < n + 2.$$

Therefore, if $(v_0, v_1, v_2) = \Lambda_n(x, y)$, we have $0 \leq v_0 \leq v_1 \leq v_2 \leq n + 1$. Also

$$\beta^{-1}x + y + \beta^* + 1 < \beta^{-1} + 1 + \beta^* + 1 = 1 + 1 = 2.$$

Thus

$$v_1 = \lfloor \beta^{-1}x + y + \beta^* + 1 \rfloor \leq 1.$$

We conclude $\Lambda_n(x, y) = (v_0, v_1, v_2) \in V_n$. □

The following lemma shows a relation between Λ_n and the map θ_n defined in the previous section in Equation (5.1).

Lemma 7.2. *If $x, y \in [0, 1)$, then*

$$\Lambda_n(x, y) = \theta_n(\Lambda_n(\{x + \beta^*\}, y), \Lambda_n(\{y + \beta^*\}, x)).$$

Proof. Let $x, y \in [0, 1)$. We want to show that if $\ell_0, \ell_1, \ell_2, b_0, b_1, b_2 \in \mathbb{Z}$ are such that

$$\Lambda_n(\{x + \beta^*\}, y) = \begin{pmatrix} \lfloor y + \beta^* + 1 \rfloor \\ \lfloor \beta^{-1}\{x + \beta^*\} + y + \beta^* + 1 \rfloor \\ \lfloor \beta\{x + \beta^*\} + y + \beta^* + 1 \rfloor \end{pmatrix} = \begin{pmatrix} \ell_0 \\ \ell_1 \\ \ell_2 \end{pmatrix}$$

and

$$\Lambda_n(\{y + \beta^*\}, x) = \begin{pmatrix} \lfloor x + \beta^* + 1 \rfloor \\ \lfloor \beta^{-1}\{y + \beta^*\} + x + \beta^* + 1 \rfloor \\ \lfloor \beta\{y + \beta^*\} + x + \beta^* + 1 \rfloor \end{pmatrix} = \begin{pmatrix} b_0 \\ b_1 \\ b_2 \end{pmatrix},$$

then $\Lambda_n(x, y) = \theta_n((\ell_0, \ell_1, \ell_2), (b_0, b_1, b_2))$. Let $r_0, r_1, r_2 \in \mathbb{Z}$ be such that

$$\Lambda_n(x, y) = \begin{pmatrix} \lfloor y + \beta^* + 1 \rfloor \\ \lfloor \beta^{-1}x + y + \beta^* + 1 \rfloor \\ \lfloor \beta x + y + \beta^* + 1 \rfloor \end{pmatrix} = \begin{pmatrix} r_0 \\ r_1 \\ r_2 \end{pmatrix}.$$

We want to show that the variables satisfy the definition of the function θ_n given in Equation (5.1). We have $r_0 = \lfloor y + \beta^* + 1 \rfloor = \ell_0$. Therefore, the first equation defining the map θ_n is satisfied.

Assume that $\ell_0 = \lfloor y + \beta^* + 1 \rfloor = 0$. Then $-\beta^{-1} = \beta^* \leq y + \beta^* < 0$. Also $0 \leq \beta^{-1}x < \beta^{-1}$. Thus $-\beta^{-1} \leq \beta^{-1}x + y + \beta^* < \beta^{-1}$. We have

$$\begin{aligned} r_1 &= \lfloor \beta^{-1}x + y + \beta^* \rfloor + 1 \\ &= \lfloor \beta(\beta^{-1}x + y + \beta^*) \rfloor + 1 && \text{(because } -\beta^{-1} \leq \beta^{-1}x + y + \beta^* < \beta^{-1}\text{)} \\ &= \lfloor \beta(y + \beta^*) + x \rfloor + 1 \\ &= \lfloor \beta(y + \beta^* + 1) + x + \beta^* \rfloor + 1 - n && \text{(because } \beta + \beta^* = n\text{)} \\ &= \lfloor \beta\{y + \beta^*\} + x + \beta^* \rfloor + 1 - n \\ &= b_2 - n \end{aligned}$$

Assume that $\ell_0 = \lfloor y + \beta^* + 1 \rfloor = 1$. Then $0 \leq y + \beta^* < 1$. Also, we have $y < 1$, so that $y + \beta^* < 1 + \beta^*$. Moreover, $0 \leq \beta^{-1}x < \beta^{-1}$. Thus, $0 < \beta^{-1}x + y + \beta^* < \beta^{-1} + 1 + \beta^* = 1$. We have

$$r_1 = \lfloor \beta^{-1}x + y + \beta^* \rfloor + 1 = 0 + 1 = \ell_0.$$

Therefore, the second equation defining the map θ_n is satisfied.

Assume that $b_0 = \lfloor x + \beta^* + 1 \rfloor = 0$. This implies that $-1 \leq x + \beta^* < 0$, which implies $x < \beta^{-1}$. Thus $0 \leq \beta x < 1$. We need to consider the cases $\ell_0 = 0$ and $\ell_0 = 1$ separately. First, suppose that $\ell_0 = \lfloor y + \beta^* + 1 \rfloor = 0$. Then $-1 \leq y + \beta^* < 0$. Thus $-1 \leq \beta x + y + \beta^* < 1$. We have

$$\begin{aligned} r_2 &= \lfloor \beta x + y + \beta^* + 1 \rfloor \\ &= \lfloor \beta^{-1}(\beta x + y + \beta^*) \rfloor + 1 && \text{(because } -1 \leq (\beta x + y + \beta^*) < 1\text{)} \\ &= \lfloor \beta^{-1}(\beta x + y + \beta^*) + \beta^{-1} + \beta^* \rfloor + 1 \\ &= \lfloor \beta^{-1}(1 + y + \beta^*) + x + \beta^* \rfloor + 1 \\ &= \lfloor \beta^{-1}\{y + \beta^*\} + x + \beta^* \rfloor + 1 \\ &= b_1 = b_1 + 0 = b_1 + \ell_0. \end{aligned}$$

Secondly, suppose that $\ell_0 = \lfloor y + \beta^* + 1 \rfloor = 1$. Then $0 \leq y + \beta^* < 1$, which implies $\{y + \beta^*\} = y + \beta^*$. Thus $0 \leq \beta x + y + \beta^* < 2$. We have

$$\begin{aligned} r_2 &= \lfloor \beta x + y + \beta^* + 1 \rfloor \\ &= \lfloor \beta x + y + \beta^* - 1 \rfloor + 2 \\ &= \lfloor \beta^{-1}(\beta x + y + \beta^* - 1) \rfloor + 2 && \text{(because } -1 \leq (\beta x + y + \beta^* - 1) < 1\text{)} \\ &= \lfloor \beta^{-1}(y + \beta^*) + x + \beta^* \rfloor + 2 \\ &= \lfloor \beta^{-1}\{y + \beta^*\} + x + \beta^* \rfloor + 2 \\ &= b_1 + 1 = b_1 + \ell_0. \end{aligned}$$

Assume that $b_0 = \lfloor x + \beta^* + 1 \rfloor = 1$. This implies that $0 \leq x + \beta^* < 1$, which implies $\{x + \beta^*\} = x + \beta^*$. We have

$$\begin{aligned} r_2 &= \lfloor \beta x + y + \beta^* + 1 \rfloor \\ &= \lfloor \beta x + \beta \beta^* + 1 + y + \beta^* + 1 \rfloor && \text{(because } \beta \beta^* = -1) \\ &= \lfloor \beta(x + \beta^*) + y + \beta^* + 1 \rfloor + 1 \\ &= \lfloor \beta\{x + \beta^*\} + y + \beta^* + 1 \rfloor + 1 \\ &= \ell_2 + 1 = \ell_2 + b_1. \end{aligned}$$

Therefore, the third equation defining the map θ_n is satisfied. \square

For every $(x, y) \in \mathbb{R}^2$, let

$$\text{TILE}_n(x, y) = (\Lambda_n(\{x\}, \{y\}), \Lambda_n(\{y\}, \{x\}), \Lambda_n(\{x + \beta^*\}, \{y\}), \Lambda_n(\{y + \beta^*\}, \{x\}))$$

which can be interpreted geometrically as a Wang tile:

$$\text{TILE}_n(x, y) = \begin{array}{ccc} & \Lambda_n(\{y\}, \{x\}) & \\ \Lambda_n(\{x + \beta^*\}, \{y\}) & \square & \Lambda_n(\{x\}, \{y\}) \\ & \Lambda_n(\{y + \beta^*\}, \{x\}) & \end{array}$$

Lemma 7.3. *If $(x, y) \in \mathbb{R}^2$, then*

- $\text{TILE}_n(x, y) \in (V_n)^4$,
- $\text{TILE}_n(x, y) \in \mathcal{C}_n$ is an instance of a θ_n -chip tile.

Proof. From Lemma 7.1, for every $(x, y) \in [0, 1)^2$, we have $\Lambda_n(x, y) \in V_n$. Therefore, for every $(x, y) \in \mathbb{R}^2$,

$$\Lambda_n(\{x\}, \{y\}), \Lambda_n(\{y\}, \{x\}), \Lambda_n(\{x + \beta^*\}, \{y\}), \Lambda_n(\{y + \beta^*\}, \{x\}) \in V_n.$$

From Lemma 7.2, for every $(x, y) \in \mathbb{R}^2$, we have

$$\Lambda_n(\{x\}, \{y\}) = \theta_n(\Lambda_n(\{x + \beta^*\}, \{y\}), \Lambda_n(\{y + \beta^*\}, \{x\})).$$

Also

$$\Lambda_n(\{y\}, \{x\}) = \theta_n(\Lambda_n(\{y + \beta^*\}, \{x\}), \Lambda_n(\{x + \beta^*\}, \{y\})).$$

Thus $\text{TILE}_n(x, y) \in \mathcal{C}_n$. \square

Here is another characterization of the set of Wang tiles \mathcal{T}_n .

Proposition 7.4. *The following holds:*

$$\mathcal{T}_n = \{ \text{TILE}_n(x, y) : (x, y) \in [0, 1)^2 \}.$$

Proof. First, recall from Proposition 5.1 that

$$(7.1) \quad \mathcal{C}_n = \mathcal{T}'_n = \mathcal{T}_n \cup \{j_n^{0,0,1,1}, j_n^{1,1,0,0}\} \cup \{a_n^i, \widehat{a}_n^i \mid 1 \leq i \leq n\} \cup \{b_n^n, \widehat{b}_n^n\}$$

where

$$\{j_n^{0,0,1,1}, j_n^{1,1,0,0}\} = \left\{ \begin{array}{cc} \begin{array}{ccc} & 011 & \\ 01\bar{n} & \begin{array}{c} \text{X} \\ \text{tile} \end{array} & 000 \\ & 00n & \end{array} & \begin{array}{ccc} & 000 & \\ 00n & \begin{array}{c} \text{X} \\ \text{tile} \end{array} & 011 \\ & 01\bar{n} & \end{array} \end{array} \right\}.$$

Let

$$U_n = \{ \text{TILE}_n(x, y) : (x, y) \in [0, 1)^2 \}.$$

First we show that $U_n \subseteq \mathcal{T}_n$. It follows from Lemma 7.3 that $U_n \subset \mathcal{C}_n$. Thus, using Equation (7.1), the goal is to show that

$$(7.2) \quad U_n \cap \left(\{j_n^{0,0,1,1}, j_n^{1,1,0,0}\} \cup \{a_n^i, \widehat{a}_n^i \mid 1 \leq i \leq n\} \cup \{b_n^n, \widehat{b}_n^n\} \right) = \emptyset.$$

Suppose that there exists $(x, y) \in [0, 1]^2$ such that $\text{TILE}_n(x, y) = j_n^{0,0,1,1}$. Then $\Lambda_n(x, y) = 000$ and $\Lambda_n(y, x) = 011$. More precisely, we have

$$\begin{aligned} \Lambda_n(x, y) &= \begin{pmatrix} \lfloor y + \beta^* + 1 \rfloor \\ \lfloor \beta^{-1}x + y + \beta^* + 1 \rfloor \\ \lfloor \beta x + y + \beta^* + 1 \rfloor \end{pmatrix} = \begin{pmatrix} 0 \\ 0 \\ 0 \end{pmatrix}, \\ \Lambda_n(y, x) &= \begin{pmatrix} \lfloor x + \beta^* + 1 \rfloor \\ \lfloor \beta^{-1}y + x + \beta^* + 1 \rfloor \\ \lfloor \beta y + x + \beta^* + 1 \rfloor \end{pmatrix} = \begin{pmatrix} 0 \\ 1 \\ 1 \end{pmatrix}. \end{aligned}$$

In particular,

$$0 = \lfloor \beta x + y + \beta^* + 1 \rfloor \geq \lfloor \beta^{-1}y + x + \beta^* + 1 \rfloor = 1,$$

which is a contradiction. The same contradiction is obtained if $\text{TILE}_n(x, y) = j_n^{1,1,0,0}$. Therefore, these two junction tiles are not in U_n .

Suppose that there exists $(x, y) \in [0, 1]^2$ such that $\text{TILE}_n(x, y) = a_n^i$ for some integer i satisfying $1 \leq i \leq n$. Then $\Lambda_n(x, y) = 00\bar{i}$ and $\Lambda_n(y, x) = 112$. More precisely, we have

$$\begin{aligned} \Lambda_n(x, y) &= \begin{pmatrix} \lfloor y + \beta^* + 1 \rfloor \\ \lfloor \beta^{-1}x + y + \beta^* + 1 \rfloor \\ \lfloor \beta x + y + \beta^* + 1 \rfloor \end{pmatrix} = \begin{pmatrix} 0 \\ 0 \\ i + 1 \end{pmatrix}, \\ \Lambda_n(y, x) &= \begin{pmatrix} \lfloor x + \beta^* + 1 \rfloor \\ \lfloor \beta^{-1}y + x + \beta^* + 1 \rfloor \\ \lfloor \beta y + x + \beta^* + 1 \rfloor \end{pmatrix} = \begin{pmatrix} 1 \\ 1 \\ 2 \end{pmatrix}. \end{aligned}$$

In particular, $\lfloor y + \beta^* + 1 \rfloor = 0$ implies that $-\beta^{-1} \leq y + \beta^* < 0$. Also $0 \leq \beta^{-1}x < \beta^{-1}$, so that $-\beta^{-1} \leq \beta^{-1}x + y + \beta^* < \beta^{-1}$. Therefore,

$$0 = \lfloor \beta^{-1}x + y + \beta^* + 1 \rfloor = \lfloor \beta(\beta^{-1}x + y + \beta^*) \rfloor + 1 = \lfloor \beta y + x - 1 \rfloor + 1 = \lfloor \beta y + x \rfloor.$$

On the other hand, using $\lfloor a + b \rfloor \leq \lfloor a \rfloor + \lfloor b \rfloor + 1$ for every $a, b \in \mathbb{R}$, we obtain

$$2 = \lfloor \beta y + x + \beta^* + 1 \rfloor \leq \lfloor \beta y + x \rfloor + \lfloor \beta^* + 1 \rfloor + 1 = 0 + 0 + 1 = 1,$$

which is a contradiction. A similar contradiction is obtained if we suppose that such that $\text{TILE}_n(x, y) = \widehat{a}_n^i$. Therefore, there is no antigreen tile in U_n .

Suppose that there exists $(x, y) \in [0, 1]^2$ such that $\text{TILE}_n(x, y) = b_n^n$. Then $\Lambda_n(x, y) = 00\bar{n}$ and $\Lambda_n(y, x) = 111$. More precisely, we have

$$\Lambda_n(x, y) = \begin{pmatrix} \lfloor y + \beta^* + 1 \rfloor \\ \lfloor \beta^{-1}x + y + \beta^* + 1 \rfloor \\ \lfloor \beta x + y + \beta^* + 1 \rfloor \end{pmatrix} = \begin{pmatrix} 0 \\ 0 \\ n + 1 \end{pmatrix}.$$

In particular, using $\beta = n + \beta^{-1}$ and $x < 1$, we obtain

$$\begin{aligned} n + 1 &= \lfloor \beta x + y + \beta^* + 1 \rfloor \\ &= \lfloor (n + \beta^{-1})x + y + \beta^* + 1 \rfloor \\ &\leq \lfloor n + \beta^{-1}x + y + \beta^* + 1 \rfloor \\ &= \lfloor \beta^{-1}x + y + \beta^* + 1 \rfloor + n = 0 + n = n, \end{aligned}$$

which is a contradiction. A similar contradiction is obtained if we suppose that such that $\text{TILE}_n(x, y) = \widehat{b}_n^n$. Therefore, the blue tiles b_n^n and \widehat{b}_n^n are not in U_n . This shows that Equation (7.2) holds. Thus $U_n \subseteq \mathcal{T}_n$.

Now we show that $\mathcal{T}_n \subseteq U_n$. We have $J_n \subset U_n$ since

$$\begin{aligned} j_n^{0,0,0,0} &= \text{TILE}_n(0, 0), \\ j_n^{0,1,0,0} &= \text{TILE}_n(\beta^{-2}, 0), \\ j_n^{0,0,0,1} &= \text{TILE}_n(0, \beta^{-2}), \\ j_n^{0,1,0,1} &= \text{TILE}_n\left(\frac{1}{\beta(\beta+1)}, \frac{1}{\beta(\beta+1)}\right), \\ j_n^{1,1,0,1} &= \text{TILE}_n(x, y), \text{ where } (x, y) \text{ is on the segment from } (0, \beta^{-1}) \text{ to } ((\beta+1)^{-1}, (\beta+1)^{-1}), \\ j_n^{0,1,1,1} &= \text{TILE}_n(x, y) \text{ where } (x, y) \text{ is on the segment from } (\beta^{-1}, 0) \text{ to } ((\beta+1)^{-1}, (\beta+1)^{-1}), \\ j_n^{1,1,1,1} &= \text{TILE}_n\left(\frac{1}{\beta+1}, \frac{1}{\beta+1}\right). \end{aligned}$$

We have $B_n \subset U_n$ since

$$\begin{aligned} b_n^0 &= \text{TILE}_n(\beta^{-1}, 0), \\ b_n^i &= \text{TILE}_n(\beta^{-2} + \beta^{-1}i, 0) \text{ for every integer } i \text{ with } 1 \leq i \leq n-1, \\ \widehat{b}_n^0 &= \text{TILE}_n(0, \beta^{-1}), \\ \widehat{b}_n^i &= \text{TILE}_n(0, \beta^{-2} + \beta^{-1}i) \text{ for every integer } i \text{ with } 1 \leq i \leq n-1. \end{aligned}$$

We have $G_n \subset U_n$ since

$$\begin{aligned} g_n^0 &= \text{TILE}_n(\beta^{-1}, \beta^{-2}(\beta-1)) \\ g_n^i &= \text{TILE}_n\left(\frac{i}{n}, \beta^{-1}(1 - \frac{i}{n})\right) \text{ for every integer } i \text{ with } 1 \leq i \leq n, \\ \widehat{g}_n^0 &= \text{TILE}_n(\beta^{-2}(\beta-1), \beta^{-1}) \\ \widehat{g}_n^i &= \text{TILE}_n\left(\beta^{-1}(1 - \frac{i}{n}), \frac{i}{n}\right) \text{ for every integer } i \text{ with } 1 \leq i \leq n. \end{aligned}$$

We have $Y_n \subset U_n$ since

$$\begin{aligned} y_n^1 &= \text{TILE}_n(\beta^{-1} + \varepsilon, \beta^{-1} - \varepsilon\beta^{-1}) \text{ for some small } \varepsilon > 0, \\ y_n^i &= \text{TILE}_n\left(\frac{i-\beta^{-2}}{n}, \frac{\beta^{-1}}{n}(n-i+\beta^{-1}-\beta^{-2})\right) \text{ for every integer } i \text{ with } 2 \leq i \leq n, \\ \widehat{y}_n^1 &= \text{TILE}_n(\beta^{-1} - \varepsilon\beta^{-1}, \beta^{-1} + \varepsilon) \text{ for some small } \varepsilon > 0, \\ \widehat{y}_n^i &= \text{TILE}_n\left(\frac{\beta^{-1}}{n}(n-i+\beta^{-1}-\beta^{-2}), \frac{i-\beta^{-2}}{n}\right) \text{ for every integer } i \text{ with } 2 \leq i \leq n. \end{aligned}$$

We have $W_n \subset U_n$ since

$$\begin{aligned} w_n^{1,1} &= \text{TILE}_n(\beta^{-1}, \beta^{-1}), \\ w_n^{1,j} &= \text{TILE}_n(\beta^{-1}, j\beta^{-1} - \beta^{-2}) \text{ for every integer } j \text{ with } 2 \leq j \leq n, \\ w_n^{i,1} &= \text{TILE}_n(i\beta^{-1} - \beta^{-2}, \beta^{-1}) \text{ for every integer } i \text{ with } 2 \leq i \leq n, \\ w_n^{i,j} &= \text{TILE}_n\left(\beta^{-1} + \frac{1}{n}((i-1) - (j-1)\beta^{-1}), \beta^{-1} + \frac{1}{n}((j-1) - (i-1)\beta^{-1})\right) \\ &\quad \text{for every integer } i, j \text{ with } 2 \leq i, j \leq n. \end{aligned}$$

Therefore $\mathcal{T}_n = W_n \cup Y_n \cup G_n \cup B_n \cup J_n \subseteq U_n$. We conclude that $\mathcal{T}_n = U_n$. \square

$\text{TILE}_n \left(\begin{matrix} x - \frac{1}{\beta} \\ y + \frac{2}{\beta} \end{matrix} \right)$	$\text{TILE}_n \left(\begin{matrix} x \\ y + \frac{2}{\beta} \end{matrix} \right)$	$\text{TILE}_n \left(\begin{matrix} x + \frac{1}{\beta} \\ y + \frac{2}{\beta} \end{matrix} \right)$	$\text{TILE}_n \left(\begin{matrix} x + \frac{2}{\beta} \\ y + \frac{2}{\beta} \end{matrix} \right)$
$\text{TILE}_n \left(\begin{matrix} x - \frac{1}{\beta} \\ y + \frac{1}{\beta} \end{matrix} \right)$	$\text{TILE}_n \left(\begin{matrix} x \\ y + \frac{1}{\beta} \end{matrix} \right)$	$\text{TILE}_n \left(\begin{matrix} x + \frac{1}{\beta} \\ y + \frac{1}{\beta} \end{matrix} \right)$	$\text{TILE}_n \left(\begin{matrix} x + \frac{2}{\beta} \\ y + \frac{1}{\beta} \end{matrix} \right)$
$\text{TILE}_n \left(\begin{matrix} x - \frac{1}{\beta} \\ y \end{matrix} \right)$	$\text{TILE}_n \left(\begin{matrix} x \\ y \end{matrix} \right)$	$\text{TILE}_n \left(\begin{matrix} x + \frac{1}{\beta} \\ y \end{matrix} \right)$	$\text{TILE}_n \left(\begin{matrix} x + \frac{2}{\beta} \\ y \end{matrix} \right)$
$\text{TILE}_n \left(\begin{matrix} x - \frac{1}{\beta} \\ y - \frac{1}{\beta} \end{matrix} \right)$	$\text{TILE}_n \left(\begin{matrix} x \\ y - \frac{1}{\beta} \end{matrix} \right)$	$\text{TILE}_n \left(\begin{matrix} x + \frac{1}{\beta} \\ y - \frac{1}{\beta} \end{matrix} \right)$	$\text{TILE}_n \left(\begin{matrix} x + \frac{2}{\beta} \\ y - \frac{1}{\beta} \end{matrix} \right)$

FIGURE 14. For every $(x, y) \in [0, 1]^2$ the map $\mathbb{Z}^2 \rightarrow \mathcal{T}_n$ defined by $(i, j) \mapsto \text{TILE}_n(x + \frac{i}{\beta}, y + \frac{j}{\beta})$ is a valid tiling of the plane by the set of Wang tiles \mathcal{T}_n .

This allows to construct valid configurations $\mathbb{Z}^2 \rightarrow \mathcal{T}_n$ from any starting point (x, y) on the torus. For every $(x, y) \in [0, 1]^2$, let

$$c_{(x,y)} : \begin{array}{ccc} \mathbb{Z}^2 & \rightarrow & \mathcal{T}_n \\ (i, j) & \mapsto & \text{TILE}_n(x + i\beta^{-1}, y + j\beta^{-1}). \end{array}$$

See Figure 14.

Theorem C. *Let $n \geq 1$ be an integer. For every $(x, y) \in [0, 1]^2$, the configuration*

$$c_{(x,y)} : \mathbb{Z}^2 \rightarrow \mathcal{T}_n$$

is a valid tiling of the plane by the set of metallic mean Wang tiles \mathcal{T}_n .

Proof. Let $(x, y) \in [0, 1]^2$ and $(i, j) \in \mathbb{Z}^2$. We have $c_{(x,y)}(i, j) \in \mathcal{T}_n$ from Proposition 7.4. Also the right color of the tile $c_{(x,y)}(i, j)$ is equal to the left color of the tile $c_{(x,y)}(i + 1, j)$ and the top color of the tile $c_{(x,y)}(i, j)$ is equal to the bottom color of the tile $c_{(x,y)}(i, j + 1)$. Therefore, $c_{(x,y)}$ is a valid configuration of Wang tiles from the set \mathcal{T}_n . \square

The set $\{c_{(x,y)} : (x, y) \in [0, 1]^2\}$ is not a subshift because it is not topologically closed. Indeed, if (x_0, y_0) lies on the boundary of the partition, there is more than one configuration associated with it. The configuration $c_{(x_0, y_0)}$ is one of them, but $\lim_{(x,y) \rightarrow (x_0, y_0)} c_{(x,y)}$ might be a different configuration if the limit is taken coming from another direction. The same issue happens with the

representation of numbers in base 10. For example, the number 1 has two base-10 representations, one being $1.000000\dots$ and the other $0.999999\dots$. One way to solve this issue is to take the topological closure

$$C = \overline{\{c_{(x,y)} : (x,y) \in [0,1]^2\}}$$

which is a subshift satisfying $C \subseteq \Omega_n$. A cleaner way of creating this subshift is to construct the symbolic dynamical system defined from a dynamical system on a space together with a partition of the space. This is what we do in the next section.

8. AN EXPLICIT FACTOR MAP

First, it is convenient to make some observation on the inner product with the vector $d = (0, -1, 1)$ of the tile labels.

Lemma 8.1. *Let $n \geq 1$ be an integer and $d = (0, -1, 1)$. If $x, y \in [0, 1)$, then*

$$\langle d, \Lambda_n(x, y) \rangle = \lfloor nx \rfloor + \mathbb{I}_{[1-\{nx\}, 1)}(\{\delta_x + y\})$$

where $\delta_x = 1 - \beta^{-1}(1 - x)$.

Proof. Let $x, y \in [0, 1)$. Observe that $\delta_x = 1 - \beta^{-1}(1 - x) = \beta^{-1}x + \beta^* + 1$. We have

$$\begin{aligned} \langle d, \Lambda_n(x, y) \rangle &= \lfloor \beta x + y + \beta^* + 1 \rfloor - \lfloor \beta^{-1}x + y + \beta^* + 1 \rfloor \\ &= \lfloor (n + \beta^{-1})x + y + \beta^* + 1 \rfloor - \lfloor \beta^{-1}x + y + \beta^* + 1 \rfloor \\ &= \lfloor nx + \delta_x + y \rfloor - \lfloor \delta_x + y \rfloor \\ &= (\lfloor nx \rfloor + \lfloor \delta_x + y \rfloor + \lfloor \{nx\} + \{\delta_x + y\} \rfloor) - \lfloor \delta_x + y \rfloor \\ &= \lfloor nx \rfloor + \lfloor \{nx\} + \{\delta_x + y\} \rfloor \\ &= \lfloor nx \rfloor + \begin{cases} 0 & \text{if } \{nx\} + \{\delta_x + y\} < 1, \\ 1 & \text{if } \{nx\} + \{\delta_x + y\} \geq 1. \end{cases} \end{aligned}$$

The conclusion follows. □

As illustrated in Figure 5 for a finite rectangular pattern, the average of the values of $\langle \frac{1}{n}d, v \rangle$ for labels v appearing along an horizontal line can also be considered for valid configurations $w : \mathbb{Z}^2 \rightarrow \mathcal{T}_n$. For some reason, it is convenient to consider the average of the top label of the tiles on the horizontal row passing through the origin. Assuming that the limit exists for every configuration, this leads to a map from the Wang shift to the interval $[0, 1]$ defined as follows:

$$(8.1) \quad \begin{aligned} \phi_n : \Omega_n &\rightarrow [0, 1] \\ w &\mapsto \lim_{k \rightarrow \infty} \frac{1}{2k+1} \sum_{i=-k}^k \langle \frac{1}{n}d, \text{TOP}(w_{i,0}) \rangle \end{aligned}$$

where $\text{TOP}(t)$ denotes the top label of the Wang tile t .

We show in the next proposition that ϕ_n is well-defined and that it recovers the parameter y of a configuration $c_{(x,y)}$.

Proposition 8.2. *For every integer $n \geq 1$, ϕ_n is a continuous and onto map $\Omega_n \rightarrow [0, 1]$ such that*

$$\begin{aligned} \phi_n(\sigma^{e_1}w) &= \phi_n(w), \\ \phi_n(\sigma^{e_2}w) &= \phi_n(w) + \beta^{-1} \pmod{1}, \end{aligned}$$

where β is the positive root of the polynomial $x^2 - nx - 1$. Moreover, for every $(x, y) \in [0, 1)^2$, we have $\phi_n(c_{(x,y)}) = y$.

Proof. (i) Let $R_\alpha(x) = \{x + \alpha\}$ be the rotation by angle α on the interval $[0, 1)$. If α is irrational, then for every $x \in [0, 1)$ the sequence $(R_\alpha^i(x))_{i \in \mathbb{Z}}$ is uniformly distributed modulo 1 [KN74, Exercise 2.5]. Therefore, using Weyl's equidistribution theorem for Riemann-integrable functions [KN74, Corollary 1.1], we have that for every $(x, y) \in [0, 1)^2$, we have

$$\begin{aligned}
\phi_n(c_{(x,y)}) &= \lim_{k \rightarrow \infty} \frac{1}{2k+1} \sum_{i=-k}^k \langle \frac{1}{n}d, \text{TOP}(c_{(x,y)}(i, 0)) \rangle \\
&= \lim_{k \rightarrow \infty} \frac{1}{2k+1} \sum_{i=-k}^k \langle \frac{1}{n}d, \text{TOP}(\text{TILE}_n(x + i\beta^{-1}, y)) \rangle \\
&= \lim_{k \rightarrow \infty} \frac{1}{2k+1} \sum_{i=-k}^k \langle \frac{1}{n}d, \Lambda_n(y, \{x + i\beta^{-1}\}) \rangle \\
&= \frac{1}{n} \lim_{k \rightarrow \infty} \frac{1}{2k+1} \sum_{i=-k}^k \left(\lfloor ny \rfloor + \mathbb{I}_{[1-\{ny\}, 1)}(\{\delta_y + \{x + i\beta^{-1}\}) \} \right) \quad (\text{Lemma 8.1}) \\
&= \frac{1}{n} \left(\lfloor ny \rfloor + \lim_{k \rightarrow \infty} \frac{1}{2k+1} \sum_{i=-k}^k \mathbb{I}_{[1-\{ny\}, 1)}(R_{\beta^{-1}}^i(\delta_y + x)) \right) \\
&= \frac{1}{n} \left(\lfloor ny \rfloor + \int_0^1 \mathbb{I}_{[1-\{ny\}, 1)}(t) dt \right) \quad (\text{Weyl's equidistribution theorem}) \\
&= \frac{1}{n} (\lfloor ny \rfloor + \{ny\}) = \frac{1}{n}(ny) = y.
\end{aligned}$$

(ii) Now we want to show that the rule ϕ_n defines a continuous map $\Omega_n \rightarrow \mathbb{T}$. Since Ω_n is minimal [Lab23a], we have that the orbit $\overline{\{c_{(0,0)}\}^\sigma} = \{\sigma^k c_{(0,0)} \mid k \in \mathbb{Z}^2\} = \{c_{\beta^{-1}k \pmod{\mathbb{Z}^2}} \mid k \in \mathbb{Z}^2\}$ is a dense subset of Ω_n . Therefore $\{c_{(x,y)} \mid x, y \in [0, 1)\}$ is dense in Ω_n . Let $w \in \Omega_n$. There exists a sequence $(x^{(\ell)}, y^{(\ell)})_{\ell \in \mathbb{N}}$ with $x^{(\ell)}, y^{(\ell)} \in [0, 1)$ such that $w = \lim_{\ell \rightarrow \infty} c_{(x^{(\ell)}, y^{(\ell)})}$.

Notice that the limit $(x^{(\infty)}, y^{(\infty)}) = \lim_{\ell \rightarrow \infty} (x^{(\ell)}, y^{(\ell)}) \in [0, 1]^2$ exist. This essentially follows from [Lab21a, Lemma 3.4] allowing to define another factor map, see Equation (9.2). Indeed, suppose on the contrary that the sequence $(x^{(\ell)}, y^{(\ell)})_{\ell \in \mathbb{N}}$ has two distinct accumulation points (p_1, q_1) and (p_2, q_2) . Recall that $\{\text{Interior}(\text{TILE}_n^{-1}(t))\}_{t \in \mathcal{T}_n}$ is a topological partition of \mathbb{T}^2 . Since the orbits under the \mathbb{Z}^2 -action R_n are dense, there exists $(i, j) \in \mathbb{Z}^2$ such that $R_n^{(i,j)}(p_1, q_1) \in \text{Interior}(\text{TILE}_n^{-1}(t_1))$ and $R_n^{(i,j)}(p_2, q_2) \in \text{Interior}(\text{TILE}_n^{-1}(t_2))$ where t_1 and t_2 are two distinct tiles in \mathcal{T}_n . Therefore for sufficiently large $\ell \in \mathbb{N}$, we have

$$\begin{aligned}
w(i, j) &= c_{(x^{(\ell)}, y^{(\ell)})}(i, j) = \text{TILE}_n(R_n^{(i,j)}(p_1, q_1)) = t_1, \\
w(i, j) &= c_{(x^{(\ell)}, y^{(\ell)})}(i, j) = \text{TILE}_n(R_n^{(i,j)}(p_2, q_2)) = t_2,
\end{aligned}$$

which is a contradiction.

We split the proof according to the behavior of $\lim_{\ell \rightarrow \infty} ny^{(\ell)}$, and more precisely if it converges to an integer and if so from above or from below (the fact that it converge from above or from below if it converges to an integer follows from the existence of the configuration w because the boundary of the topological partition $\{\text{Interior}(\text{TILE}_n^{-1}(t))\}_{t \in \mathcal{T}_n}$ contains the vertical and horizontal lines passing through integers points). We proceed as above using Weyl equidistribution theorem. We have

$$\phi_n(w) = \phi_n \left(\lim_{\ell \rightarrow \infty} c_{(x^{(\ell)}, y^{(\ell)})} \right)$$

$$\begin{aligned}
&= \lim_{k \rightarrow \infty} \frac{1}{2k+1} \sum_{i=-k}^k \lim_{\ell \rightarrow \infty} \langle \frac{1}{n} d, \text{TOP}(c_{(x^{(\ell)}, y^{(\ell)})}(i, 0)) \rangle \\
&= \frac{1}{n} \lim_{k \rightarrow \infty} \frac{1}{2k+1} \sum_{i=-k}^k \lim_{\ell \rightarrow \infty} \left(\lfloor ny^{(\ell)} \rfloor + \mathbb{I}_{[1-\{ny^{(\ell)}\}, 1)}(\{\delta_{y^{(\ell)}} + \{x^{(\ell)} + i\beta^{-1}\}) \right) \\
&= \frac{1}{n} \lim_{k \rightarrow \infty} \frac{1}{2k+1} \sum_{i=-k}^k \lim_{\ell \rightarrow \infty} \left(\lfloor ny^{(\ell)} \rfloor + \mathbb{I}_{[1-\{ny^{(\ell)}\}, 1]}(R_{\beta^{-1}}^i(\delta_{y^{(\ell)}} + x^{(\ell)})) \right) \\
&= \begin{cases} \frac{1}{n} \lim_{k \rightarrow \infty} \frac{1}{2k+1} \sum_{i=-k}^k \left(\lfloor ny^{(\infty)} \rfloor + \mathbb{I}_{\emptyset}(R_{\beta^{-1}}^i(\delta_{y^{(\infty)}} + x^{(\infty)})) \right) & \text{if } \{ny^{(\ell)}\} \rightarrow 0, \\ \frac{1}{n} \lim_{k \rightarrow \infty} \frac{1}{2k+1} \sum_{i=-k}^k \left(\lfloor ny^{(\infty)} \rfloor - 1 + \mathbb{I}_{(0,1)}(R_{\beta^{-1}}^i(\delta_{y^{(\infty)}} + x^{(\infty)})) \right) & \text{if } \{ny^{(\ell)}\} \rightarrow 1, \\ \frac{1}{n} \lim_{k \rightarrow \infty} \frac{1}{2k+1} \sum_{i=-k}^k \left(\lfloor ny^{(\infty)} \rfloor + \mathbb{I}_{[1-\{ny^{(\infty)}\}, 1]}(R_{\beta^{-1}}^i(\delta_{y^{(\infty)}} + x^{(\infty)})) \right) & \text{if } \{ny^{(\ell)}\} \not\rightarrow 0, 1, \end{cases} \\
&= \begin{cases} \frac{1}{n} \left(\lfloor ny^{(\infty)} \rfloor + \int_0^1 \mathbb{I}_{\emptyset}(t) dt \right) & \text{if } \{ny^{(\ell)}\} \rightarrow 0, \\ \frac{1}{n} \left(\lfloor ny^{(\infty)} \rfloor - 1 + \int_0^1 \mathbb{I}_{(0,1)}(t) dt \right) & \text{if } \{ny^{(\ell)}\} \rightarrow 1, \\ \frac{1}{n} \left(\lfloor ny^{(\infty)} \rfloor + \int_0^1 \mathbb{I}_{[1-\{ny^{(\infty)}\}, 1]}(t) dt \right) & \text{if } \{ny^{(\ell)}\} \not\rightarrow 0, 1, \end{cases} \\
&= \begin{cases} \frac{1}{n} \lfloor ny^{(\infty)} \rfloor + 0 & \text{if } \{ny^{(\ell)}\} \rightarrow 0, \\ \frac{1}{n} \lfloor ny^{(\infty)} \rfloor - 1 + 1 & \text{if } \{ny^{(\ell)}\} \rightarrow 1, \\ \frac{1}{n} \left(\lfloor ny^{(\infty)} \rfloor + \{ny^{(\infty)}\} \right) & \text{if } \{ny^{(\ell)}\} \not\rightarrow 0, 1, \end{cases} \\
&= y^{(\infty)} = \lim_{\ell \rightarrow \infty} y^{(\ell)} = \lim_{\ell \rightarrow \infty} \phi_n(c_{(x^{(\ell)}, y^{(\ell)})}).
\end{aligned}$$

This shows that the rule ϕ_n defines a map $\Omega_n \rightarrow [0, 1]$ and that this map is continuous.

(iii) If $y \in [0, 1)$, then $y = \phi_n(c_{(0,y)})$. If $y = 1$, then $y = \phi_n(\lim_{y \rightarrow 1^-} c_{(0,y)})$. Thus, the map ϕ_n is onto.

(iv) Since the map ϕ_n is continuous, we only need to show the equalities for a dense subset of Ω_n . Let $(x, y) \in [0, 1)^2$. We have

$$\phi_n(\sigma^{e_1} c_{(x,y)}) = \phi_n(c_{(\{x+\beta^{-1}\}, y)}) = y = \phi_n(c_{(x,y)}).$$

Moreover, we have

$$\phi_n(\sigma^{e_2} c_{(x,y)}) = \phi_n(c_{(x, \{y+\beta^{-1}\})}) = \{y + \beta^{-1}\} = \phi_n(c_{(x,y)}) + \beta^{-1} \pmod{1}. \quad \square$$

Since $\phi_n(\sigma^{e_1} w) = \phi_n(w)$ for every configuration $w \in \Omega_n$, the factor map ϕ_n is far from being injective. We may improve this as follows. We use the symmetry of the tiles in \mathcal{T}_n to define an involution on Ω_n . If $w \in \Omega_n$ is a configuration, then its image under a reflection by the positive diagonal is the configuration $\hat{w} \in \Omega_n$ defined as

$$\hat{w} : \begin{array}{ccc} \mathbb{Z}^2 & \rightarrow & \mathcal{T}_n \\ (i, j) & \mapsto & \widehat{w_{j,i}}. \end{array}$$

This allows to define a map from the Wang shift to the 2-dimensional torus

$$(8.2) \quad \begin{array}{ccc} \Phi_n : \Omega_n & \rightarrow & \mathbb{T}^2 \\ w & \mapsto & (\phi_n(\hat{w}), \phi_n(w)). \end{array}$$

The first coordinate $\phi_n(\hat{w})$ computes the average of the inner product with d of the right labels of the Wang tiles in the column containing the origin of the configuration w . We show in the next proposition that Φ_n is a factor map.

Theorem D. *Let $n \geq 1$ be an integer and Ω_n be the n^{th} metallic mean Wang shift. The map $\Phi_n : \Omega_n \rightarrow \mathbb{T}^2$ is a factor map, that is, it is continuous, onto and commutes the shift $\mathbb{Z}^2 \curvearrowright \Omega_n$*

with the toral \mathbb{Z}^2 -rotation $\mathbb{Z}^2 \stackrel{R_n}{\curvearrowright} \mathbb{T}^2$ by the equation $\Phi_n \circ \sigma^k = R_n^k \circ \Phi_n$ for every $k \in \mathbb{Z}^2$ where

$$\begin{aligned} R_n &: \mathbb{Z}^2 \times \mathbb{T}^2 \rightarrow \mathbb{T}^2 \\ (k, x) &\mapsto R_n^k(x) := x + \beta k \end{aligned}$$

and $\beta = \frac{n+\sqrt{n^2+4}}{2}$ is the n^{th} metallic mean, that is, the positive root of the polynomial $x^2 - nx - 1$.

Proof. From Proposition 8.2, ϕ_n is continuous and onto. Thus Φ_n is also a continuous and onto map. Let $w \in \Omega_n$ be a configuration. Let $k = (k_1, k_2) \in \mathbb{Z}^2$. Using Proposition 8.2, we have

$$\begin{aligned} \Phi_n \circ \sigma^k(w) &= (\phi_n(\widehat{\sigma^k w}), \phi_n(\sigma^k w)) \\ &= (\phi_n(\sigma^{(k_2, k_1)} \widehat{w}), \phi_n(\sigma^{(k_1, k_2)} w)) \\ &= (\phi_n(\widehat{w}) + \beta^{-1} k_1, \phi_n(w) + \beta^{-1} k_2) \pmod{\mathbb{Z}^2} \\ &= (\phi_n(\widehat{w}), \phi_n(w)) + \beta^{-1} (k_1, k_2) \pmod{\mathbb{Z}^2} \\ &= \Phi_n(w) + \beta^{-1} k \pmod{\mathbb{Z}^2} \\ &= R_n^k \circ \Phi_n(w). \end{aligned} \quad \square$$

9. ISOMORPHISM WITH A TORAL \mathbb{Z}^2 -ROTATION

The goal of this section is to show more properties of the factor map $\Phi_n : \Omega_n \rightarrow \mathbb{T}^2$ introduced in the previous section. Based on the approach presented in [Lab21a], we prove Theorem E and Theorem F.

Let $n \geq 1$ be an integer. We consider the continuous \mathbb{Z}^2 -action R_n defined on $\mathbb{T}^2 = \mathbb{R}^2/\mathbb{Z}^2$ by

$$\begin{aligned} R_n &: \mathbb{Z}^2 \times \mathbb{T}^2 \rightarrow \mathbb{T}^2 \\ (\mathbf{n}, \mathbf{x}) &\mapsto R_n^{\mathbf{n}}(\mathbf{x}) := \mathbf{x} + \beta \mathbf{n} \end{aligned}$$

where $\beta = \frac{n+\sqrt{n^2+4}}{2}$ is the positive root of the polynomial $x^2 - nx - 1$. We say that R_n is a **toral \mathbb{Z}^2 -rotation** and it defines a dynamical system that we denote $\mathbb{Z}^2 \stackrel{R_n}{\curvearrowright} \mathbb{T}^2$. In this section, we encode this dynamical system symbolically using a partition associated with the Wang tiles \mathcal{T}_n .

Recall that

$$\begin{aligned} \Lambda_n &: [0, 1)^2 \rightarrow \mathbb{Z}^3 \\ (x, y) &\mapsto \begin{pmatrix} \lfloor y + \beta^* + 1 \rfloor \\ \lfloor \beta^{-1}x + y + \beta^* + 1 \rfloor \\ \lfloor \beta x + y + \beta^* + 1 \rfloor \end{pmatrix}. \end{aligned}$$

From Lemma 7.1, we have in fact that Λ_n is a map $[0, 1)^2 \rightarrow V_n$. Therefore,

$$\text{EAST}_n = \{\Lambda_n^{-1}(v) : v \in V_n\}$$

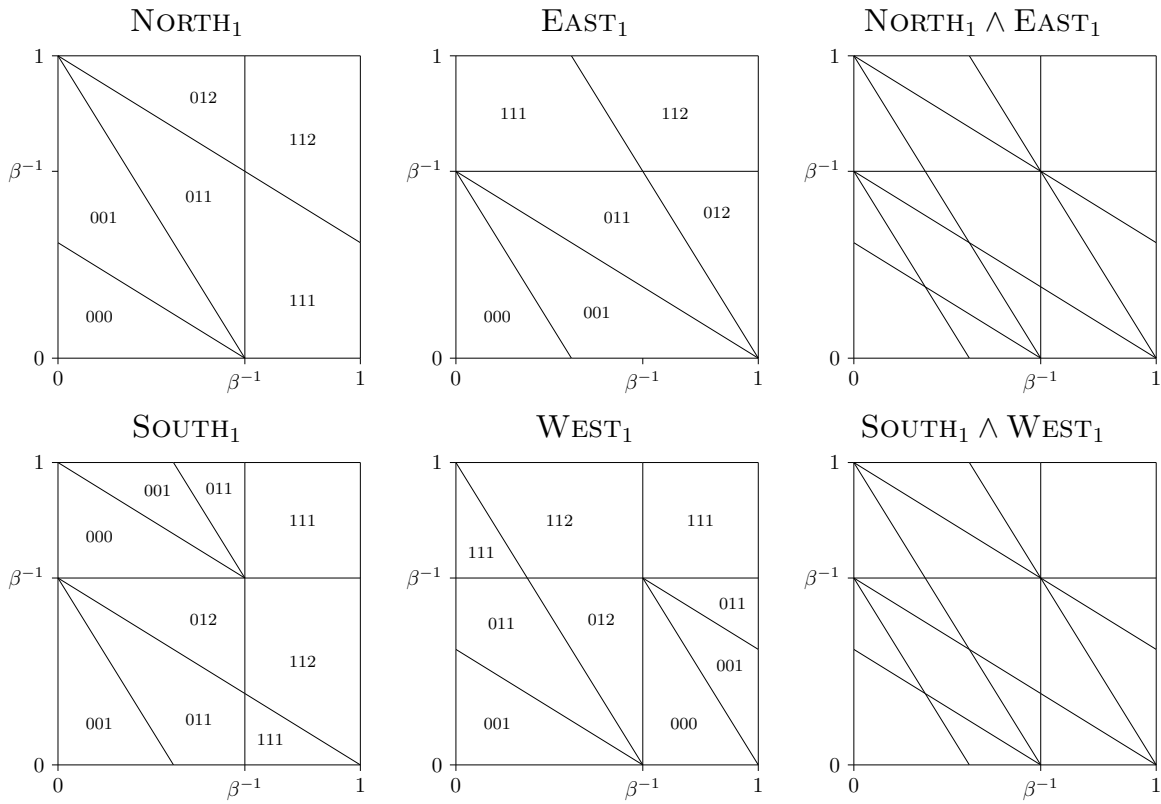
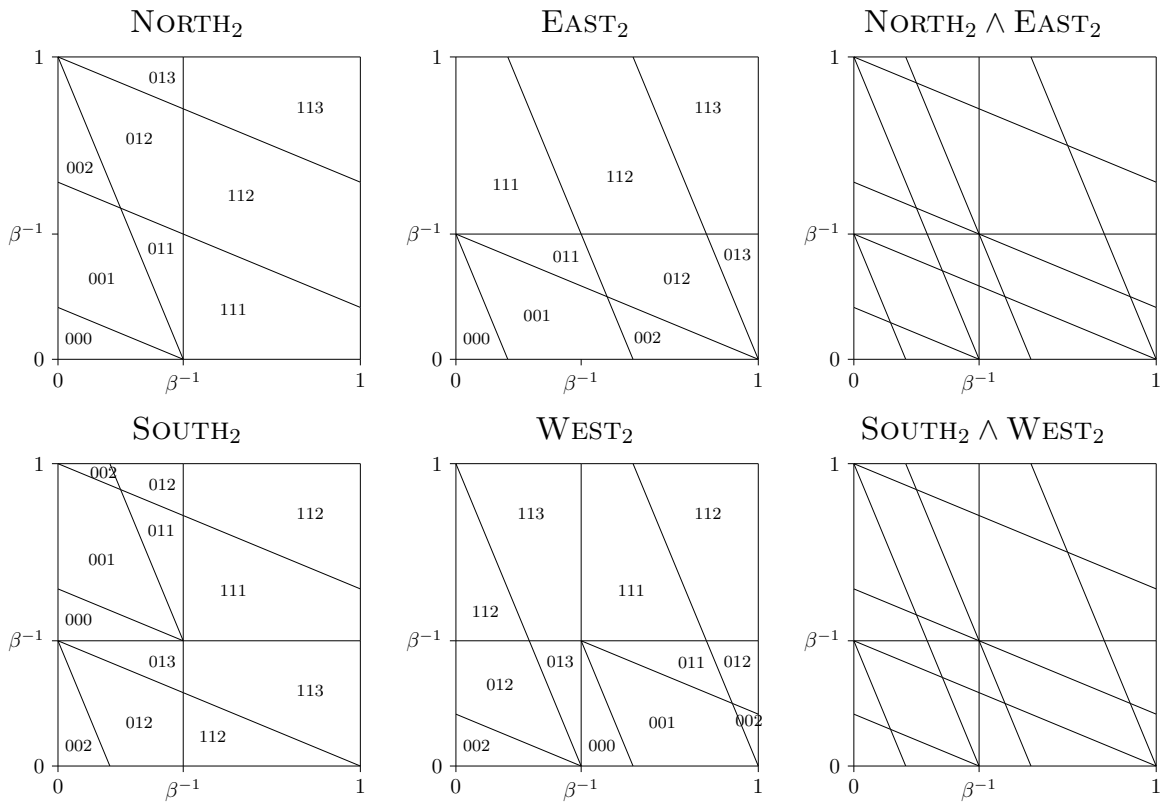
is a partition of $[0, 1)^2$. Its symmetric image is

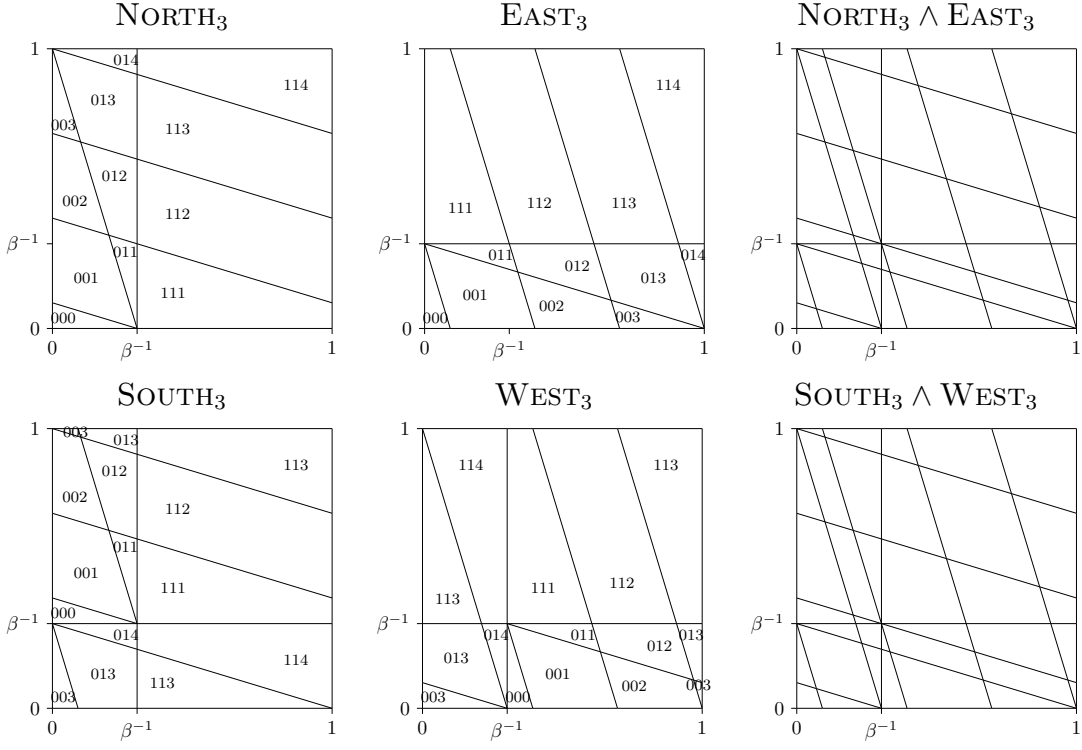
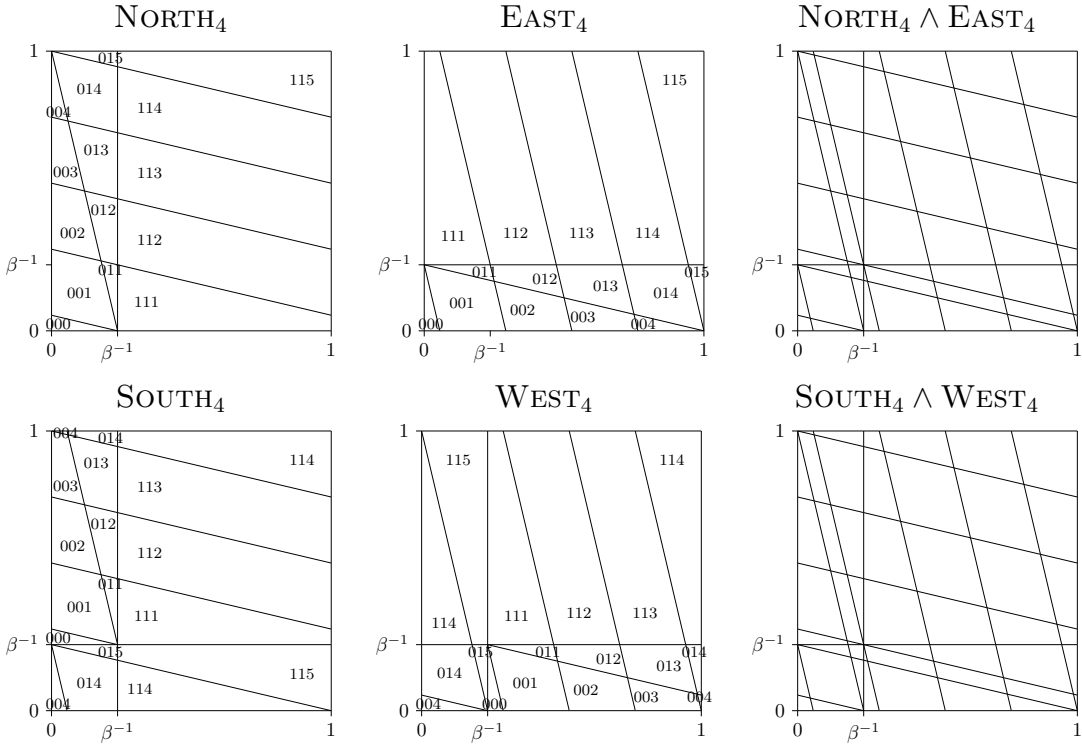
$$\text{NORTH}_n = \{\eta \circ \Lambda_n^{-1}(v) : v \in V_n\}$$

which is another partition of $[0, 1)^2$, where $\eta : (x, y) \mapsto (y, x)$. Also, we let

$$\begin{aligned} \text{WEST}_n &= R_n^{\mathbf{e}_1}(\text{EAST}_n), \\ \text{SOUTH}_n &= R_n^{\mathbf{e}_2}(\text{NORTH}_n) \end{aligned}$$

where $\mathbf{e}_1 = (1, 0)$ and $\mathbf{e}_2 = (0, 1)$. These partitions are illustrated for $n = 1, 2, 3, 4$ in Figure 15, Figure 16, Figure 17 and Figure 18. We may observe in these figures a nice property of the partitions: $\text{EAST}_n \wedge \text{NORTH}_n$ is the same partition (with different indices) as $\text{WEST}_n \wedge \text{SOUTH}_n$.

FIGURE 15. The partitions $NORTH_1$, $EAST_1$, $SOUTH_1$ and $WEST_1$.FIGURE 16. The partitions $NORTH_2$, $EAST_2$, $SOUTH_2$ and $WEST_2$.


 FIGURE 17. The partitions NORTH_3 , EAST_3 , SOUTH_3 and WEST_3 .

 FIGURE 18. The partitions NORTH_4 , EAST_4 , SOUTH_4 and WEST_4 .

We now want to construct the refined partition $\text{EAST}_n \wedge \text{NORTH}_n \wedge \text{WEST}_n \wedge \text{SOUTH}_n$ whose atoms are defined as follows. For each $(v_1, v_2, v_3, v_4) \in (V_n)^4$, we define the interior of the intersection

$$P_{(v_1, v_2, v_3, v_4)} = \text{Interior} \left(\Lambda_n^{-1}(v_1) \cap \eta \circ \Lambda_n^{-1}(v_2) \cap R^{e_1}(\Lambda_n^{-1}(v_3)) \cap R^{e_2}(\eta \circ \Lambda_n^{-1}(v_4)) \right).$$

It follows from Proposition 7.4 that the quadruples τ for which P_τ has nonempty interior define a set which is equal to the set of Wang tiles \mathcal{T}_n :

$$\mathcal{T}_n = \left\{ \tau \in (V_n)^4 \mid P_\tau \neq \emptyset \right\}.$$

Naturally, this comes with a topological partition

$$\mathcal{P}_n = \{P_\tau\}_{\tau \in \mathcal{T}_n}$$

of $\mathbb{R}^2/\mathbb{Z}^2$ which is the refinement of the four partitions EAST_n (the right color), NORTH_n (the top color), WEST_n (the left color) and SOUTH_n (the bottom color). Recall that, for some finite set A , a **topological partition** of a compact metric space M is a finite collection $\{P_a\}_{a \in A}$ of disjoint open sets $P_a \subset M$ such that $M = \bigcup_{a \in A} \overline{P_a}$.

9.1. Symbolic dynamical system $\mathcal{X}_{\mathcal{P}_n, R_n}$. We now define the symbolic dynamical system associated with the toral \mathbb{Z}^2 -rotation R_n generated by the partition \mathcal{P}_n . We adapt [LM95] to the 2-dimensional setting as it was done in [Hoc16] and [Lab21a].

If $S \subset \mathbb{Z}^2$ is a finite set, we say that a pattern $w \in \mathcal{A}^S$ is **allowed** for \mathcal{P}_n, R_n if

$$(9.1) \quad \bigcap_{k \in S} R_n^{-k}(P_{w_k}) \neq \emptyset.$$

Let $\mathcal{L}_{\mathcal{P}_n, R_n}$ be the collection of all allowed patterns for \mathcal{P}_n, R_n . The set $\mathcal{L}_{\mathcal{P}_n, R_n}$ is the language of a subshift $\mathcal{X}_{\mathcal{P}_n, R_n} \subseteq \mathcal{A}^{\mathbb{Z}^2}$ defined as follows, see [Hoc16, Prop. 9.2.4],

$$\mathcal{X}_{\mathcal{P}_n, R_n} = \{x \in \mathcal{A}^{\mathbb{Z}^2} \mid \pi_S \circ \sigma^n(x) \in \mathcal{L}_{\mathcal{P}_n, R_n} \text{ for every } n \in \mathbb{Z}^2 \text{ and finite subset } S \subset \mathbb{Z}^2\}.$$

We say that $\mathcal{X}_{\mathcal{P}_n, R_n}$ is the **symbolic dynamical system** corresponding to \mathcal{P}_n, R_n .

For each $w \in \mathcal{X}_{\mathcal{P}_n, R_n} \subset \mathcal{A}^{\mathbb{Z}^2}$ and $m \geq 0$ there is a corresponding nonempty open set

$$D_m(w) = \bigcap_{\|k\| \leq m} R_n^{-k}(P_{w_k}) \subseteq \mathbb{T}^2.$$

The closures $\overline{D}_m(w)$ of these sets are compact and decrease with n , so that $\overline{D}_0(w) \supseteq \overline{D}_1(w) \supseteq \overline{D}_2(w) \supseteq \dots$. It follows that $\bigcap_{m=0}^{\infty} \overline{D}_m(w) \neq \emptyset$. In order for points in $\mathcal{X}_{\mathcal{P}_n, R_n}$ to correspond to points in \mathbb{T}^2 , this intersection should contain only one point. This leads to the following definition.

A topological partition \mathcal{P}_n of \mathbb{T}^2 **gives a symbolic representation** of $\mathbb{Z}^2 \overset{R_n}{\curvearrowright} \mathbb{T}^2$ if for every $w \in \mathcal{X}_{\mathcal{P}_n, R_n}$ the intersection $\bigcap_{m=0}^{\infty} \overline{D}_m(w)$ consists of exactly one point $x \in \mathbb{T}^2$. We call w a **symbolic representation of x** .

Markov partitions were originally defined for one-dimensional dynamical systems $\mathbb{Z} \overset{T}{\curvearrowright} \mathbb{T}^2$ and were extended to \mathbb{Z}^d -actions by automorphisms of compact Abelian group in [ES97]. Following [Lab21a, Lab21b], we use the same terminology and extend the definition proposed in [LM95, §6.5] for dynamical systems defined by higher-dimensional actions by rotations.

Definition 9.1. *A topological partition \mathcal{P} of \mathbb{T}^2 is a **Markov partition** for $\mathbb{Z}^2 \overset{R}{\curvearrowright} \mathbb{T}^2$ if*

- \mathcal{P} gives a symbolic representation of $\mathbb{Z}^2 \overset{R}{\curvearrowright} \mathbb{T}^2$ and
- $\mathcal{X}_{\mathcal{P}, R}$ is a shift of finite type (SFT).

9.2. Proofs of main results. First, we have the following result.

Lemma 9.2. *The dynamical system $\mathbb{Z}^2 \overset{\sigma}{\curvearrowright} \mathcal{X}_{\mathcal{P}_n, R_n}$ is minimal and $\mathcal{X}_{\mathcal{P}_n, R_n}$ is aperiodic.*

Proof. Since $R_n^{e_1}$ and $R_n^{e_2}$ are linearly independent irrational rotations on $\mathbb{R}^2/\mathbb{Z}^2$, we have that R_n is a free \mathbb{Z}^2 -action. Thus from [Lab21a, Lemma 5.2], $\mathcal{X}_{\mathcal{P}_n, R_n}$ is minimal and aperiodic. \square

Each atom of the partition \mathcal{P}_n is invariant only under the trivial translation. Therefore, from [Lab21a, Lemma 3.4], \mathcal{P}_n gives a symbolic representation of the dynamical system $\mathbb{Z}^2 \xrightarrow{R_n} \mathbb{T}^2$. Thus we can define the following function:

$$(9.2) \quad f_n : \mathcal{X}_{\mathcal{P}_n, R_n} \rightarrow \mathbb{T}^2$$

be such that $f_n(w)$ is the unique point in the intersection $\bigcap_{m=0}^{\infty} \overline{D}_m(w)$.

Proposition 9.3. *Let $n \geq 1$ be an integer. The map $f_n : \mathcal{X}_{\mathcal{P}_n, R_n} \rightarrow \mathbb{T}^2$ is a factor map satisfying*

$$\Phi_n \circ \sigma^k = R_n^k \circ \Phi_n$$

for every $k \in \mathbb{Z}^2$.

Proof. The result is an application of Proposition 5.1 from [Lab21a]. \square

From the minimality of the Wang shift Ω_n proved separately in [Lab23a], we may now prove Theorem F using the same method as in [Lab21a].

Theorem F. *For every integer $n \geq 1$, the symbolic dynamical system $\mathcal{X}_{\mathcal{P}_n, R_n}$ corresponding to \mathcal{P}_n, R_n is equal to the metallic mean Wang shift Ω_n :*

$$\mathcal{X}_{\mathcal{P}_n, R_n} = \Omega_n.$$

In particular, \mathcal{P}_n is a Markov partition for the dynamical system $\mathbb{Z}^2 \xrightarrow{R_n} \mathbb{T}^2$.

Proof. From Proposition 8.1 in [Lab21a], we have that $\mathcal{X}_{\mathcal{P}_n, R_n} \subseteq \Omega_n$ for every integer $n \geq 1$. It was proved in [Lab23a] that the Wang shift Ω_n is minimal for every integer $n \geq 1$. Thus $\mathcal{X}_{\mathcal{P}_n, R_n} = \Omega_n$.

Each atom of the partition \mathcal{P}_n is invariant only under the trivial translation. Therefore, from [Lab21a, Lemma 3.4], \mathcal{P}_n gives a symbolic representation of $\mathbb{Z}^2 \xrightarrow{R_n} \mathbb{T}^2$. Since $\mathcal{X}_{\mathcal{P}_n, R_n} = \Omega_n$ is a shift of finite type, we conclude that the partition \mathcal{P}_n is a Markov partition for the dynamical system $\mathbb{Z}^2 \xrightarrow{R_n} \mathbb{T}^2$. \square

We can show many dynamical properties about the \mathbb{Z}^2 -action R_n on the torus \mathbb{T}^2 . Its proof follows the structure of a similar result proved in [Lab21a] for Jeandel–Rao tilings.

Theorem E. *The Wang shift Ω_n and the \mathbb{Z}^2 -action R_n have the following properties:*

- (i) $\mathbb{Z}^2 \xrightarrow{R_n} \mathbb{T}^2$ is the maximal equicontinuous factor of $\mathbb{Z}^2 \xrightarrow{\sigma} \Omega_n$,
- (ii) the factor map $\Omega_n \rightarrow \mathbb{T}^2$ is almost one-to-one and its set of fiber cardinalities is $\{1, 2, 8\}$,
- (iii) the dynamical system $\mathbb{Z}^2 \xrightarrow{\sigma} \Omega_n$ is strictly ergodic and the measure-preserving dynamical system $(\Omega_n, \mathbb{Z}^2, \sigma, \nu)$ is isomorphic to $(\mathbb{T}^2, \mathbb{Z}^2, R_n, \lambda)$ where ν is the unique shift-invariant probability measure on Ω_n and λ is the Haar measure on \mathbb{T}^2 .

Proof. From Theorem F, we have $\mathcal{X}_{\mathcal{P}_n, R_n} = \Omega_n$.

(i) From Proposition 9.3, the factor map $f_n : \mathcal{X}_{\mathcal{P}_n, R_n} \rightarrow \mathbb{T}^2$ commutes the actions $\mathbb{Z}^2 \xrightarrow{\sigma} \mathcal{X}_{\mathcal{P}_n, R_n}$ and $\mathbb{Z}^2 \xrightarrow{R_n} \mathbb{T}^2$. From [Lab21a, Proposition 5.1], f_n is one-to-one on $f_n^{-1}(\mathbb{T}^2 \setminus \Delta_{\mathcal{P}_n, R_n})$ where

$$\Delta_{\mathcal{P}_n, R_n} := \bigcup_{\mathbf{k} \in \mathbb{Z}^2} R_n^{\mathbf{k}} \left(\bigcup_{\tau \in \mathcal{T}_n} \partial P_{\tau} \right) \subset \mathbb{T}^2$$

is the set of points whose orbit under the \mathbb{Z}^2 -action R_n intersect the boundary of the topological partition $\mathcal{P}_n = \{P_{\tau}\}_{\tau \in \mathcal{T}_n}$. From [Lab21a, Corollary 5.3] (which is a consequence of [ABKL15, Lemma 3.11]), $\mathbb{Z}^2 \xrightarrow{R_n} \mathbb{T}^2$ is the maximal equicontinuous factor of $\mathbb{Z}^2 \xrightarrow{\sigma} \mathcal{X}_{\mathcal{P}_n, R_n}$.

(ii) We have that $\{y \in \mathbb{T}^2 : \text{card}(f_n^{-1}(y)) = 1\} = \mathbb{T}^2 \setminus \Delta_{\mathcal{P}_n, R_n}$ is a countable intersection of open sets and is dense in \mathbb{T}^2 . Thus it is a G_δ -dense set in \mathbb{T}^2 . Therefore, the factor map $f_n : \mathcal{X}_{\mathcal{P}_n, R_n} \rightarrow \mathbb{T}^2$ is almost one-to-one.

Suppose that $\mathbf{x} \in \Delta_{\mathcal{P}_n, R_n}$. We have $\text{card}(f_n^{-1}(\mathbf{x})) \geq 2$. If $\text{card}(f_n^{-1}(\mathbf{x})) > 2$, then we may show that there exists $\mathbf{n} \in \mathbb{Z}^2$ such that $\mathbf{x} = R_n^n(\mathbf{0})$. If $\mathbf{x} = R_n^n(\mathbf{0})$ for some $\mathbf{n} \in \mathbb{Z}^2$, then the set $f_n^{-1}(\mathbf{x})$ contains 8 different configurations of the form $\lim_{\varepsilon \rightarrow 0} c_{\varepsilon \mathbf{v}}$ for some $\mathbf{v} \in \mathbb{R}^2 \setminus \Theta^{\mathcal{P}_n}$ where $\Theta^{\mathcal{P}_n} = \mathbb{R} \cdot \{(1, 0), (0, 1), (1, -\beta), (1, \beta^*)\}$. If $\mathbf{x} \in \Delta_{\mathcal{P}_n, R_n}$ but not in the orbit of $\mathbf{0}$ under R_n , then $\text{card}(f_n^{-1}(\mathbf{x})) = 2$. We conclude that $\{\text{card}(f_n^{-1}(\mathbf{x})) \mid \mathbf{x} \in \mathbb{T}^2\} = \{1, 2, 8\}$.

(iii) We have that $\lambda(\partial P) = 0$ for each atom $P \in \mathcal{P}_n$ where λ is the Haar measure on \mathbb{T}^2 . The result follows from [Lab21a, Proposition 6.1]. \square

In fact, we can show that the factor map f_n is equal to the map Φ_n explicitly defined in Section 8 from the average of the labels of Wang tiles on the row and column containing the origin. It follows from the next lemma.

Lemma 9.4. *For every $(x, y) \in [0, 1]^2$, we have $f_n(c_{(x,y)}) = (x, y)$.*

Proof. Let $v_1, v_2, v_3, v_4 \in V_n$. Observe that

$$\begin{aligned} \text{TILE}_n^{-1}(v_1, v_2, v_3, v_4) &\subseteq \Lambda_n^{-1}(v_1) \cap \eta \circ \Lambda_n^{-1}(v_2) \cap R^{e_1}(\Lambda_n^{-1}(v_3)) \cap R^{e_2}(\eta \circ \Lambda_n^{-1}(v_4)) \\ &\subseteq \overline{\Lambda_n^{-1}(v_1) \cap \eta \circ \Lambda_n^{-1}(v_2) \cap R^{e_1}(\Lambda_n^{-1}(v_3)) \cap R^{e_2}(\eta \circ \Lambda_n^{-1}(v_4))} \\ &= \overline{P_{(v_1, v_2, v_3, v_4)}}. \end{aligned}$$

For every $k \in \mathbb{Z}^2$, we have

$$c_{(x,y)}(k) = \text{TILE}_n \circ R_n^k(x, y),$$

so that

$$(x, y) \in R_n^{-k} \circ \text{TILE}_n^{-1}(c_{(x,y)}(k)) \subset R_n^{-k}(\overline{P_{c_{(x,y)}(k)}}).$$

Therefore, for every $m \in \mathbb{N}$, we have

$$(x, y) \in \bigcap_{\|k\| \leq m} R_n^{-k}(\overline{P_{c_{(x,y)}(k)}}) = \overline{D_m}(c_{(x,y)}).$$

Since \mathcal{P}_n gives a symbolic representation of the dynamical system $\mathbb{Z}^2 \xrightarrow{R_n} \mathbb{T}^2$, we have that $\bigcap_{m=0}^{\infty} \overline{D_m}(c_{(x,y)})$ is a singleton and

$$\bigcap_{m=0}^{\infty} \overline{D_m}(c_{(x,y)}) = \{(x, y)\}.$$

Therefore $f(c_{(x,y)}) = (x, y)$. \square

Theorem 9.5. *The factor map $f_n : \Omega_n \rightarrow \mathbb{T}^2$ is equal to the factor map $\Phi_n : \Omega_n \rightarrow \mathbb{T}^2$ explicitly defined in Equation (8.2):*

$$f_n = \Phi_n.$$

Proof. From Lemma 9.4, we have $f_n(c_{(0,0)}) = (0, 0)$. Also, observe that the configuration $c_{(0,0)}$ is symmetric: $\widehat{c_{(0,0)}} = c_{(0,0)}$. Thus, we have

$$\Phi_n(c_{(0,0)}) = (\phi_n(\widehat{c_{(0,0)}}), \phi_n(c_{(0,0)})) = (\phi_n(c_{(0,0)}), \phi_n(c_{(0,0)})) = (0, 0).$$

Let $w \in \Omega_n$ be any configuration. Since Ω_n is minimal [Lab23a], there exists a sequence $(k_\ell)_{\ell \in \mathbb{N}}$ such that $k_\ell \in \mathbb{Z}^2$ such that $w = \lim_{\ell \rightarrow \infty} \sigma^{k_\ell}(c_{(0,0)})$. From Proposition 9.3 and Theorem D, f_n and

Φ_n are factor maps commuting the shift map with the \mathbb{Z}^2 -action R_n on the torus \mathbb{T}^2 . Thus, we obtain

$$\begin{aligned}
\Phi_n(w) &= \Phi_n \left(\lim_{\ell \rightarrow \infty} \sigma^{k_\ell}(c_{(0,0)}) \right) \\
&= \lim_{\ell \rightarrow \infty} \Phi_n \circ \sigma^{k_\ell}(c_{(0,0)}) \\
&= \lim_{\ell \rightarrow \infty} R_n^{k_\ell} \circ \Phi_n(c_{(0,0)}) \\
&= \lim_{\ell \rightarrow \infty} R_n^{k_\ell}((0,0)) \\
&= \lim_{\ell \rightarrow \infty} R_n^{k_\ell} \circ f_n(c_{(0,0)}) \\
&= \lim_{\ell \rightarrow \infty} f_n \circ \sigma^{k_\ell}(c_{(0,0)}) \\
&= f_n \left(\lim_{\ell \rightarrow \infty} \sigma^{k_\ell}(c_{(0,0)}) \right) = f_n(w). \quad \square
\end{aligned}$$

10. RENORMALIZATION AND RAUZY INDUCTION OF \mathbb{Z}^2 -ROTATIONS

Another consequence of Theorem F is that the symbolic dynamical system $\mathcal{X}_{\mathcal{P}_n, R_n}$ is self-similar because this was proved in [Lab23a] for the Wang shift Ω_n . The Rauzy induction of polygonal partitions and of toral \mathbb{Z}^2 -rotations defined in [Lab21b] can be used to compute the self-similarity of the symbolic dynamical system $\mathcal{X}_{\mathcal{P}_n, R_n}$. We illustrate below how this can be done for a fixed value of an integer $n \geq 1$.

First, we share the version of SageMath [Sag23] and optional package `slabbe` [Lab23b] used below.

```

sage: version() 1
SageMath version 10.2.rc4, Release Date: 2023-11-17 2
sage: import importlib.metadata 3
sage: importlib.metadata.version("slabbe") 4
0.7.6 5

```

We fix some positive integer $n \geq 1$. We define the positive root β of the polynomial $x^2 - nx - 1$. Computations will be done in the number field generated by this root. We perform the computations below with $n = 3$, but it works with other integers. The computation of the self-similarity for $n = 7$ from the Rauzy induction is done in about 200 seconds on a recent laptop.

```

sage: n = 3 # try with another integer, the code below works at least for 1 <= n <= 7 6
sage: x = polygen(QQ, "x") 7
sage: K.<beta> = NumberField(x^2 - n*x - 1, embedding=RR(n)) 8
sage: beta.n() 9
3.30277563773199 10

```

We define a function that computes the atoms $\Lambda_n^{-1}(v)$ for every $v \in V_n$. Note that in SageMath, an entry equal to $[-1, 7, 3, 4]$ represents the inequality $7x_1 + 3x_2 + 4x_3 \geq 1$.

```

sage: unit_square_ieqs = [[0, 1, 0], [0, 0, 1], [1, -1, 0], [1, 0, -1]] 11
sage: def Lambda_inv(a,b,c): 12
....:     ieqs = list(unit_square_ieqs) 13
....:     ieqs.extend([[ -1/beta+1-a, 0, 1], [a+1/beta, 0, -1]]) 14
....:     ieqs.extend([[ -1/beta+1-b, 1/beta, 1], [b+1/beta, -1/beta, -1]]) 15
....:     ieqs.extend([[ -1/beta+1-c, beta, 1], [c+1/beta, -beta, -1]]) 16
....:     return Polyhedron(ieqs=ieqs) 17

```

We define the set V_n and we check that the sum of the area of the polygons $\{\Lambda_n^{-1}(v)\}_{v \in V_n}$ is 1.

```
sage: Vn = [(a,b,c) for a in range(2) for b in range(2) for c in range(n+2) if a<=b<=c] 18
sage: Vn 19
[(0, 0, 0), (0, 0, 1), (0, 0, 2), (0, 0, 3), (0, 0, 4), (0, 1, 1), (0, 1, 2), (0, 1, 3), (0, 20
 1, 4), (1, 1, 1), (1, 1, 2), (1, 1, 3), (1, 1, 4)]
sage: assert sum(Lambda_inv(*v).volume() for v in Vn) == 1 21
sage: Lambda_inv(0,0,n+1).volume() # one of the atom has empty interior 22
0 23
```

For readability reason, we define a map which concatenates the entries of a vector into a string.

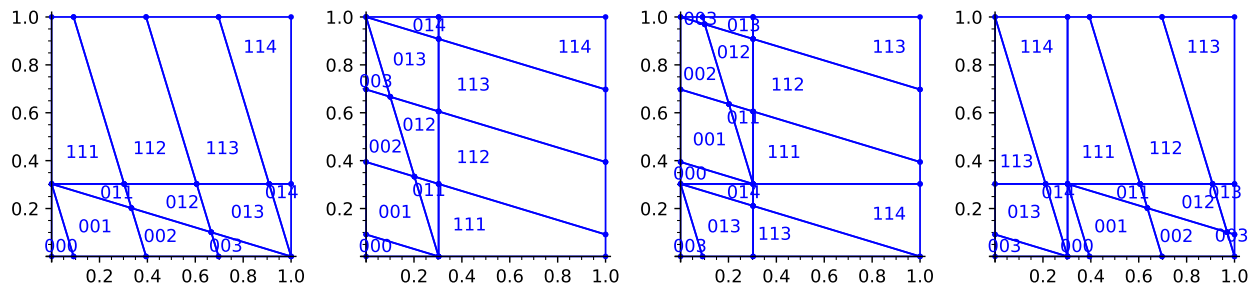
```
sage: def vector_to_str(v): 24
.....:     return "".join(str(a) for a in v) 25
sage: vector_to_str((0,1,4)) # for example 26
014 27
014 28
```

We define the \mathbb{Z}^2 -action R_n on $\mathbb{R}^2/\mathbb{Z}^2$ as two polyhedron exchange transformations on the unit square.

```
sage: lattice_base = identity_matrix(2) 28
sage: from slabbe import PolyhedronExchangeTransformation as PET 29
sage: Re1 = PET.toral_translation(lattice_base, vector((1/beta,0))) 30
sage: Re2 = PET.toral_translation(lattice_base, vector((0,1/beta))) 31
```

We construct the $EAST_n$ partition (ignoring the atom with empty interior) and the three other partitions from it.

```
sage: from slabbe import PolyhedronPartition 32
sage: EAST = PolyhedronPartition({vector_to_str(v):Lambda_inv(*v) for v in Vn 33
.....:                             if Lambda_inv(*v).volume() > 0}) 34
sage: M = matrix(K, 2, (0,1,1,0)) 35
sage: NORTH = EAST.apply_linear_map(M) 36
sage: WEST = Re1(EAST) 37
sage: SOUTH = Re2(NORTH) 38
sage: G = graphics_array([EAST.plot(),NORTH.plot(), SOUTH.plot(),WEST.plot()]) 39
sage: G.show(figsize=10) 40
None 41
```

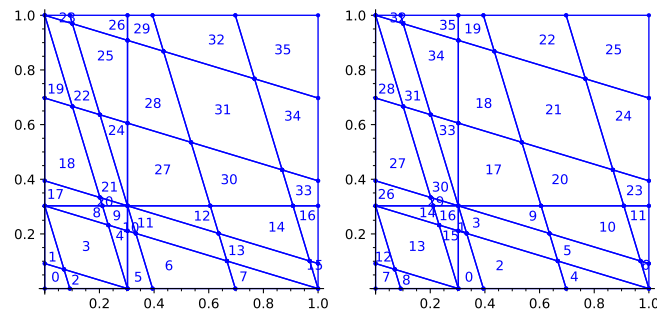


We compute the refinement of the $EAST_n$ and $NORTH_n$ partitions and of the $WEST_n$ and $SOUTH_n$ partitions.

```
sage: PEN,dEN = EAST.refinement(NORTH, certificate=True) 42
sage: PWS,dWS = WEST.refinement(SOUTH, certificate=True) 43
sage: G = graphics_array([PEN.plot(),PWS.plot()]) 44
sage: G.show(figsize=5) 45
```


None

46

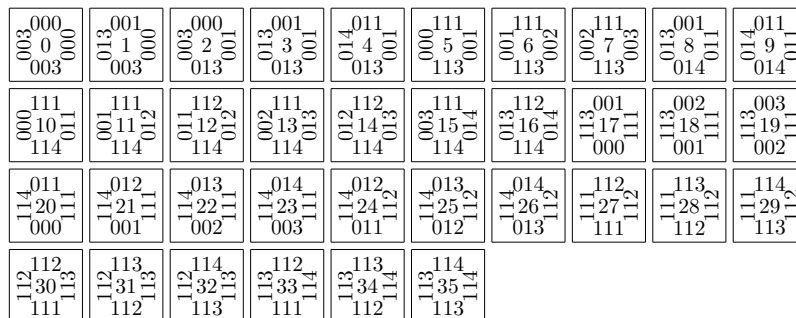


In general, we would need to compute the refinement of the two partitions. But here, since they are equal up to relabeling, we may take one as the refinement and compute the bijection of the labels between them.

```
sage: PWS.is_equal_up_to_relabeling(PEN) 47
True 48
sage: P = PEN # faster than P = PEN.refinement(PWS) 49
sage: bijection = P.keys_permutation(PWS) 50
sage: bijection[9] # for example 51
16 52
```

We compute the set of Wang tiles defined by the refinement of the four partitions $EAST_n$, $NORTH_n$, $WEST_n$ and $SOUTH_n$:

```
sage: from slabbe import WangTileSet 53
sage: tiles = [dEN[i]+dWS[bijection[i]] for i in sorted(dEN)] 54
sage: T3 = WangTileSet(tiles) 55
sage: t = T3.tikz(ncolumns=10, scale=1.2) 56
```



We perform the Rauzy induction on the square window $[0, \beta^{-1}] \times [0, \beta^{-1}]$ using the algorithms `induced_partition` and `induced_transformation` defined in [Lab21b]. First, we perform the induction the domain restricted to the inequality $x \leq \beta^{-1}$.

```
sage: x_le_beta_inv = [1/beta,-1,0] 57
sage: P1,s1 = Re1.induced_partition(x_le_beta_inv, P, substitution_type="row") 58
sage: R1e1,_ = Re1.induced_transformation(x_le_beta_inv) 59
sage: R1e2,_ = Re2.induced_transformation(x_le_beta_inv) 60
```

Secondly, we perform the induction the domain restricted to the inequality $y \leq \beta^{-1}$.

```
sage: y_le_beta_inv = [1/beta,0,-1] 61
sage: P2,s2 = Re2.induced_partition(y_le_beta_inv, P1, substitution_type="column") 62
sage: R2e1,_ = R1e1.induced_transformation(y_le_beta_inv) 63
```

```
sage: R2e2,_ = R1e2.induced_transformation(y_le_beta_inv)
```

64

We rescale the induced partition by the factor $-\beta$ and translate it back to the unit square in the positive quadrant. Then we apply each generator of the \mathbb{Z}^2 -action once on the rescaled induced partition.

```
sage: P2_scaled = (-beta * P2).translate((1,1))
```

65

```
sage: P3 = Re2(Re1(P2_scaled))
```

66

```
sage: G = graphics_array([P2_scaled.plot(), P3.plot()])
```

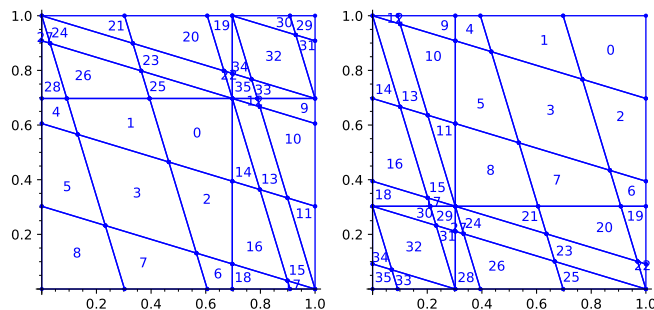
67

```
sage: G.show(figsize=5)
```

68

```
None
```

69



We check that the resulting partition is equal to the initial partition. We check that the induced action is equal to the initial action.

```
sage: P.is_equal_up_to_relabeling(P3)
```

70

```
True
```

71

```
sage: Re1 == (beta * R2e1).inverse()
```

72

```
True
```

73

```
sage: Re2 == (beta * R2e2).inverse()
```

74

```
True
```

75

The self-similarity computed by this Rauzy induction is the product of the above 2-dimensional substitutions by the bijection of the labels.

```
sage: from slabbe import Substitution2d
```

76

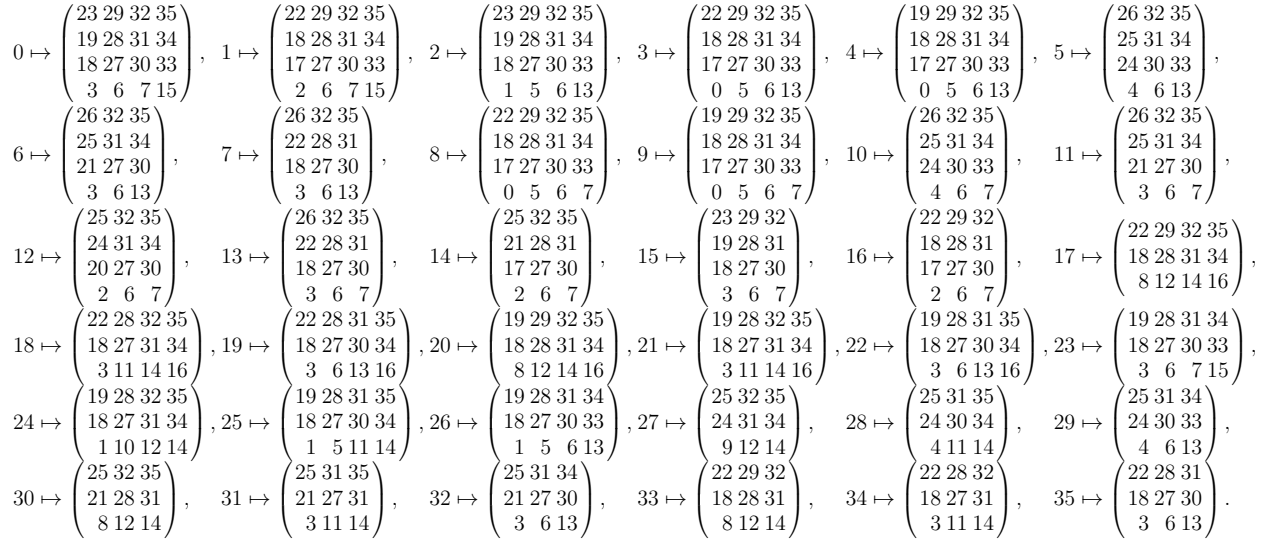
```
sage: s3 = Substitution2d.from_permutation(P.keys_permutation(P3))
```

77

```
sage: s123 = s1*s2*s3
```

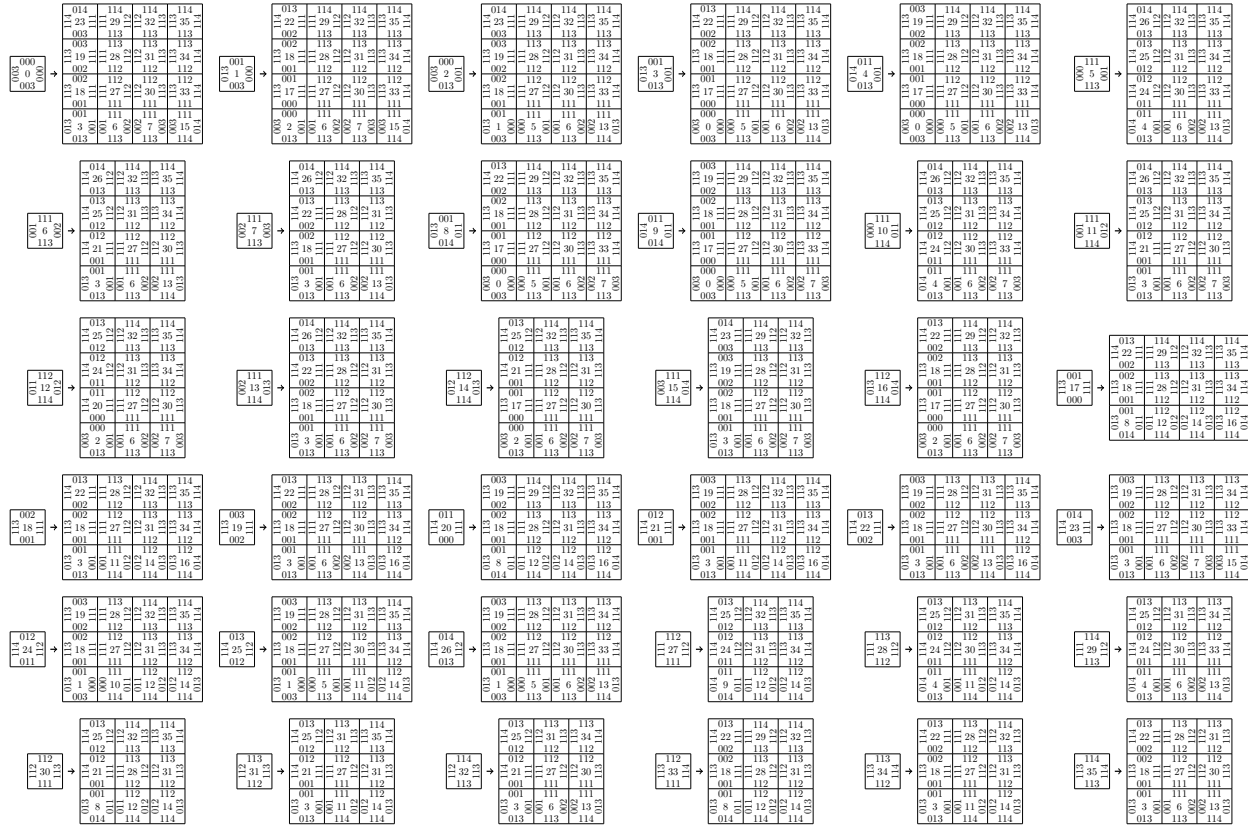
78

The computed self-similarity s_{123} is:



The above self-similarity can be illustrated with the Wang tiles computed above as follows:

```
sage: s123_tikz = s123.wang_tikz(domain_tiles=T3, codomain_tiles=T3, ncolumns=6, scale=1.2,
label_shift=.15)
```



We may observe that the self-similarity computed here from the Rauzy induction on polygonal partition on \mathcal{P}_3 and toral \mathbb{Z}^2 -action R_3 is the same as the self-similarity proved for the Wang shift Ω_3 in [Lab23a].

REFERENCES

- [AA20] Shigeki Akiyama and Pierre Arnoux, editors. *Substitution and tiling dynamics: introduction to self-inducing structures. CIRM Jean-Morlet Chair, Marseille, France, Fall 2017*, volume 2273. Cham: Springer, 2020.
- [Aar20] Scott Aaronson. The busy beaver frontier. *SIGACT News*, 51(3):32–54, sep 2020.
- [ABKL15] Jean-Baptiste Aujogue, Marcy Barge, Johannes Kellendonk, and Daniel Lenz. Equicontinuous factors, proximality and Ellis semigroup for Delone sets. In *Mathematics of Aperiodic Order*, volume 309 of *Progr. Math.*, pages 137–194. Birkhäuser/Springer, Basel, 2015.
- [AGS92] Robert Ammann, Branko Grünbaum, and G. C. Shephard. Aperiodic tiles. *Discrete Comput. Geom.*, 8(1):1–25, 1992.
- [Ber66] Robert Berger. The undecidability of the domino problem. *Mem. Amer. Math. Soc. No.*, 66:72, 1966.
- [BG13] Michael Baake and Uwe Grimm. *Aperiodic Order. Vol. 1*, volume 149 of *Encyclopedia of Mathematics and its Applications*. Cambridge University Press, Cambridge, 2013.
- [BG17] Michael Baake and Uwe Grimm, editors. *Aperiodic order. Volume 2. Crystallography and almost periodicity*, volume 166 of *Encycl. Math. Appl.* Cambridge: Cambridge University Press, 2017.
- [Bow78] Rufus Bowen. Markov partitions are not smooth. *Proc. Amer. Math. Soc.*, 71(1):130–132, 1978.
- [Bra88] Allen H. Brady. The busy beaver game and the meaning of life. The universal Turing machine, a half-century survey, 259-277 (1988)., 1988.
- [Caw91] Elise Cawley. Smooth Markov partitions and toral automorphisms. *Ergodic Theory Dynam. Systems*, 11(4):633–651, 1991.
- [Cul96] Karel Culik, II. An aperiodic set of 13 Wang tiles. *Discrete Math.*, 160(1-3):245–251, 1996.
- [DGG17] Bruno Durand, Guilhem Gamard, and Anaël Grandjean. Aperiodic tilings and entropy. *Theoret. Comput. Sci.*, 666:36–47, 2017.
- [ENP07] Stanley Eigen, Jorge Navarro, and Vidhu S. Prasad. An aperiodic tiling using a dynamical system and Beatty sequences. In *Dynamics, ergodic theory, and geometry*, volume 54 of *Math. Sci. Res. Inst. Publ.*, pages 223–241. Cambridge Univ. Press, Cambridge, 2007.
- [ES97] Manfred Einsiedler and Klaus Schmidt. Markov partitions and homoclinic points of algebraic \mathbf{Z}^d -actions. *Tr. Mat. Inst. Steklova*, 216(Din. Sist. i Smezhnye Vopr.):265–284, 1997.
- [Fie01] Doris Fiebig. Factor maps, entropy and fiber cardinality for Markov shifts. *Rocky Mountain J. Math.*, 31(3):955–986, 2001.
- [GS87] Branko Grünbaum and G. C. Shephard. *Tilings and patterns*. W. H. Freeman and Company, New York, 1987.
- [Hoc16] Michael Hochman. Multidimensional shifts of finite type and sofic shifts. In *Combinatorics, words and symbolic dynamics*, volume 159 of *Encyclopedia Math. Appl.*, pages 296–358. Cambridge Univ. Press, Cambridge, 2016.
- [Jol12] Timo Jolivet. Toral automorphisms, Markov Partitions and fractals, July 2012. https://jolivet.org/timo/docs/slides_guangzhou_toral.pdf.
- [JR21] Emmanuel Jeandel and Michaël Rao. An aperiodic set of 11 Wang tiles. *Adv. Comb.*, 2021:37, 2021. Id/No 1.
- [JV20] Emmanuel Jeandel and Pascal Vanier. The undecidability of the Domino Problem. In *Substitution and tiling dynamics: introduction to self-inducing structures*, volume 2273 of *Lecture Notes in Math.*, pages 293–357. Springer, Cham, 2020.
- [Kar96] Jarkko Kari. A small aperiodic set of Wang tiles. *Discrete Math.*, 160(1-3):259–264, 1996.
- [KN74] L. Kuipers and Harald Niederreiter. Uniform distribution of sequences. Pure and Applied Mathematics. New York etc.: John Wiley & Sons, a Wiley-Interscience Publication. xiv, 390 p. £ 13.00 (1974)., 1974.
- [Knu69] Donald E. Knuth. *The art of computer programming. Vol. 1: Fundamental algorithms*. Second printing. Addison-Wesley Publishing Co., Reading, Mass.-London-Don Mills, Ont, 1969.
- [KP99] J. Kari and P. Papasoglu. Deterministic aperiodic tile sets. *Geom. Funct. Anal.*, 9(2):353–369, 1999.
- [Kur03] Petr Kurka. *Topological and symbolic dynamics*, volume 11 of *Cours Spécialisés [Specialized Courses]*. Société Mathématique de France, Paris, 2003.
- [Lab19] Sébastien Labbé. A self-similar aperiodic set of 19 Wang tiles. *Geom. Dedicata*, 201:81–109, 2019.
- [Lab20] Sébastien Labbé. Three characterizations of a self-similar aperiodic 2-dimensional subshift. December 2020. [arxiv:2012.03892](https://arxiv.org/abs/2012.03892), 46 p., chapitre de livre en préparation.
- [Lab21a] Sébastien Labbé. Markov partitions for toral \mathbf{Z}^2 -rotations featuring Jeandel-Rao Wang shift and model sets. *Ann. H. Lebesgue*, 4:283–324, 2021.

- [Lab21b] Sébastien Labbé. Rauzy induction of polygon partitions and toral \mathbb{Z}^2 -rotations. *J. Mod. Dyn.*, 17:481–528, 2021.
- [Lab21c] Sébastien Labbé. Substitutive structure of Jeandel-Rao aperiodic tilings. *Discrete Comput. Geom.*, 65(3):800–855, 2021.
- [Lab23a] Sébastien Labbé. Metallic mean Wang tiles I: self-similarity, aperiodicity and minimality. December 2023. [arxiv:2312.03652](https://arxiv.org/abs/2312.03652).
- [Lab23b] Sébastien Labbé. Optional SageMath Package `slabbe` (Version 0.7.6). <https://pypi.python.org/pypi/slabbe/>, 2023.
- [Lin04] Douglas Lind. Multi-dimensional symbolic dynamics. In *Symbolic dynamics and its applications*, volume 60 of *Proc. Sympos. Appl. Math.*, pages 61–79. Amer. Math. Soc., Providence, RI, 2004.
- [LM95] Douglas Lind and Brian Marcus. *An Introduction to Symbolic Dynamics and Coding*. Cambridge University Press, Cambridge, 1995.
- [Moz89] Shahar Mozes. Tilings, substitution systems and dynamical systems generated by them. *J. Analyse Math.*, 53:139–186, 1989.
- [OEI23] OEIS Foundation Inc. Entry A060843 in the on-line encyclopedia of integer sequences. Busy Beaver problem: $a(n)$ = maximal number of steps that an n -state Turing machine can make on an initially blank tape before eventually halting, 2023. <https://oeis.org/A060843>.
- [Oll08] Nicolas Ollinger. Two-by-two substitution systems and the undecidability of the domino problem. In *Logic and theory of algorithms*, volume 5028 of *Lecture Notes in Comput. Sci.*, pages 476–485. Springer, Berlin, 2008.
- [Pen79] Roger Penrose. Pentaplexity. A class of non-periodic tilings of the plane. *Math. Intell.*, 2:32–37, 1979.
- [Pra99] Brenda Praggastis. Numeration systems and Markov partitions from self-similar tilings. *Trans. Amer. Math. Soc.*, 351(8):3315–3349, 1999.
- [PS01] N. Priebe and B. Solomyak. Characterization of planar pseudo-self-similar tilings. *Discrete Comput. Geom.*, 26(3):289–306, 2001.
- [Rau82] Gérard Rauzy. Nombres algébriques et substitutions. *Bull. Soc. Math. France*, 110(2):147–178, 1982.
- [Rob71] Raphael M. Robinson. Undecidability and nonperiodicity for tilings of the plane. *Invent. Math.*, 12:177–209, 1971.
- [Rob96] E. Arthur Robinson, Jr. The dynamical properties of Penrose tilings. *Trans. Amer. Math. Soc.*, 348(11):4447–4464, 1996.
- [Sag23] Sage Developers. *SageMath, the Sage Mathematics Software System (Version 10.2)*, 2023. <http://www.sagemath.org>.
- [Sch01] Klaus Schmidt. Multi-dimensional symbolic dynamical systems. In *Codes, Systems, and Graphical Models (Minneapolis, MN, 1999)*, volume 123 of *IMA Vol. Math. Appl.*, pages 67–82. Springer, New York, 2001.
- [Sen95] Marjorie Senechal. *Quasicrystals and geometry*. Cambridge: Cambridge Univ. Press, 1995.
- [Sie17] Jason Siefken. A minimal subsystem of the Kari-Culik tilings. *Ergodic Theory Dynam. Systems*, 37(5):1607–1634, 2017.
- [SMKG23a] David Smith, Joseph Samuel Myers, Craig S. Kaplan, and Chaim Goodman-Strauss. An aperiodic monotile, March 2023. [arxiv:2303.10798](https://arxiv.org/abs/2303.10798).
- [SMKG23b] David Smith, Joseph Samuel Myers, Craig S. Kaplan, and Chaim Goodman-Strauss. A chiral aperiodic monotile, May 2023. [arxiv:2305.17743](https://arxiv.org/abs/2305.17743).
- [Sol97] Boris Solomyak. Dynamics of self-similar tilings. *Ergodic Theory Dynam. Systems*, 17(3):695–738, 1997.
- [Sol98] B. Solomyak. Nonperiodicity implies unique composition for self-similar translationally finite tilings. *Discrete Comput. Geom.*, 20(2):265–279, 1998.
- [ST11] Joshua E. S. Socolar and Joan M. Taylor. An aperiodic hexagonal tile. *J. Combin. Theory Ser. A*, 118(8):2207–2231, 2011.
- [Tur36] A. M. Turing. On Computable Numbers, with an Application to the Entscheidungsproblem. *Proc. London Math. Soc. (2)*, 42(3):230–265, 1936.
- [Wal82] Peter Walters. *An Introduction to Ergodic Theory*, volume 79 of *GTM*. Springer-Verlag, New York-Berlin, 1982.
- [Wan61] Hao Wang. Proving theorems by pattern recognition – II. *Bell System Technical Journal*, 40(1):1–41, January 1961.

(S. Labbé) CNRS, LABRI, UMR 5800, F-33400 TALENCE, FRANCE
 Email address: sebastien.labbe@labri.fr
 URL: <http://www.slabbe.org/>